AGU PUBLICATIONS

JGR

Journal of Geophysical Research: Space Physics

RESEARCH ARTICLE
10.1002/2016JA023513

Special Section:
Major Results From the MAVEN Mission to Mars

Martian magnetic storms

J. G. Luhmann[1], C. F. Dong[2], Y. J. Ma[3], S. M. Curry[1], S. Xu[1], C. O. Lee[1], T. Hara[1], J. Halekas[4], Y. Li[1], J. R. Gruesbeck[5], J. Espley[5], D. A. Brain[6], C. T. Russell[3], and B. M. Jakosky[6]

[1]Space Sciences Laboratory, University of California, Berkeley, California, USA, [2]Princeton University, Princeton, New Jersey, USA, [3]Institute of Geophysics and Planetary Physics, University of California, Los Angeles, California, USA, [4]University of Iowa, Iowa City, Iowa, USA, [5]NASA Goddard Space Flight Center, Greenbelt, Maryland, USA, [6]LASP, University of Colorado Boulder, Boulder, Colorado, USA

Key Points:
- Mars has space weather storms analogous to geomagnetic storms, caused by ICMEs
- The character of these storms is unique because of the Mars-solar wind obstacle nature
- Models suggest what could happen at Mars under more extreme conditions

Correspondence to:
J. G. Luhmann,
jgluhman@ssl.berkeley.edu

Citation:
Luhmann, J. G., et al. (2017), Martian magnetic storms, *J. Geophys. Res. Space Physics*, *122*, doi:10.1002/2016JA023513.

Received 24 SEP 2016
Accepted 15 FEB 2017
Accepted article online 28 FEB 2017

Abstract The response of Mars to the major space weather events called interplanetary coronal mass ejections (ICMEs) is of interest for both general planetary solar wind interaction studies and related speculations on their evolutionary consequences—especially with respect to atmosphere escape. Various particle and field signatures of ICMEs have been observed on Phobos-2, Mars Global Surveyor (MGS), Mars Express (MEX), and now Mars Atmosphere and Volatile EvolutioN (MAVEN). Of these, MAVEN's combined instrumentation and orbit geometry is particularly well suited to characterize both the event drivers and their consequences. However, MAVEN has detected only moderate disturbances at Mars due in large part to the general weakness of the present solar cycle. Nevertheless, the strongest event observed by MAVEN in March 2015 provides an example illustrating how further insights can be gained from available models. Here we first look more closely at what previously run BATS-R-US MHD simulations of the combined MAVEN observations tell us about the March 2015 event consequences. We then use analogous models to infer those same responses, including magnetic field topology changes and ionospheric consequences, to a hypothetical extreme ICME at Mars based on STEREO A measurements in July 2012. The results suggest how greatly enhanced, yet realistic, solar wind pressure, magnetic field, and convection electric field combine to produce strong magnetospheric coupling with important consequences for upper atmosphere and ionosphere energization.

1. Introduction

Mars with its crustal magnetic fields makes a unique obstacle to the solar wind whose interaction has been studied in some detail using observations from Phobos-2, Mars Global Surveyor (MGS), and Mars Express (MEX), and now from the Mars Atmosphere and Volatile EvolutioN (MAVEN) mission. Investigations have included the influences of disturbed conditions from both solar wind stream interactions (stream interaction regions and corotating interaction regions) and interplanetary coronal mass ejections (ICMEs) [*Crider et al.*, 2005; *Edberg et al.*, 2010; *Dubinin et al.*, 2009; *Vennerstrom*, 2011; *Opgenoorth et al.*, 2013; *Morgan et al.*, 2014; *Jakosky et al.*, 2015a]. The responses to the associated enhanced upstream plasma and fields include strengthening of the draped interplanetary field piled up on the dayside of the Mars' obstacle, decreases in the dayside solar wind interaction boundary altitude, and inferred increases in planetary ion escape. To date, the reported results suggest that heavy planetary ion (e.g., O^+, O_2^+, and CO_2^+) escape rates increase by factors of ~2–10 times. However, a challenge has been to globally characterize Mars' overall reactions to truly major events, of which the largest, fasted ICMEs provide the potentially most extreme. The motivation for this lies in the potential importance of the solar wind interaction for significant loss to space, given its modest rates in the current epoch and also the knowledge that the Sun was likely more active in the past [e.g., *Jakosky et al.*, 2015b, and references therein]. At Earth we have sufficient observing resources and archives of data to have allowed relatively detailed analyses of the so-called superstorm effects in its magnetosphere and upper atmosphere. But at Mars the large events encountered during appropriately instrumented missions have occurred when either the available measurements were insufficient to characterize the event and its consequences or the observations were compromised by the event itself, e.g., intense solar energetic particle flux backgrounds [e.g., *Futaana et al.*, 2008].

Among the exceptional events encountered when spacecraft were at Mars were the March 1989 event during the Phobos-2 mission [e.g., *McKenna-Lawlor et al.*, 2005] and the so-called Halloween storms in October–November 2003 during the MGS mission [*Crider et al.*, 2005]. These events are well known in

terrestrial space weather circles because of their extreme interplanetary conditions measured upstream of the Earth, resulting in large geomagnetic and ionospheric impacts [e.g., *Vennerstrom et al.*, 2016]. The Phobos-2 observations at the time of the March 1989 event(s) were described most recently by *Aran et al.* [2007] in the context of discussing the related solar energetic particle event at Mars. They focus on 6 March 1989 when the first of a series of strong solar flares arose from a complex active region on the visible disk. Near-Earth in situ observations of the interplanetary consequences imply the interplanetary coronal ejecta traveled to 1 AU at an average speed of ~800 km/s. The same shock may have reached Mars at its location at the time 72° east of Earth (heliocentric coordinates) at 1.58 AU and have been detected there by Phobos-2 plasma and field instruments on 9 March. According to the Phobos-2 plasma and magnetic field observations [see *McKenna-Lawlor et al.*, 2005, Figure 5], the plasma speed at Mars reached ~1000 km/s on 11 March, accompanied by magnetic fields of several tens of nanoteslas and plasma densities increased by ~10 times (compared to typical pre-event values of ~2–3 nT and ~1 cm^{-3}, respectively). Another period of atypical solar wind at Mars began on 22 March with speeds ~800 km/s and similarly strong fields. *Verigin et al.* [2004] reported detections of exceptionally distant subsolar bow shock locations at this time, at the ~2.7 R_m Phobos-2 orbit, compared to the usual ~1.5 R_m position there. This greatly expanded shock phenomenon, which has also been reported at Venus under similarly disturbed solar wind conditions, is attributed to the related change in prevailing magnetosonic Mach number [*Zhang et al.*, 2008]. However, due to Phobos-2's nearly circular orbit at the distance of the moon Phobos (the primary target of the mission), the main responses of Mars itself to this apparently strong event of could not be observed.

Effects of the so-called Halloween events in late October to early November 2003 described by *Crider et al.* [2005] were measured at the much lower altitude ~400 km altitude, 2 A.M. to 2 P.M. local time mapping orbit of the Mars Global Surveyor. The most relevant observations possible with MGS included vector magnetic fields from the magnetometer [*Acuna et al.*, 1998] and suprathermal electrons from the Electron Reflectometer [*Mitchell et al.*, 2001], although backgrounds in the ER experiment also allowed related solar energetic particle (SEP) fluxes to be estimated [e.g., *Delory et al.*, 2012]. The timing of the arrival of this ICME event suggests it had an average speed ~1300 km/s en route to Mars. Using the observed magnetic field pileup on the dayside as a proxy, *Crider et al.* [2005] estimated that the incident solar wind dynamic pressure was ~7 times the normal value. Moreover, the field strength in the magnetic pileup region was over several hundred nanoteslas on the dayside on the four most affected orbits, compared to normal values for the MGS mapping mission of ~80–100 nT. Finally, the suprathermal electron data indicated that the MGS orbit was atypically in the magnetosheath nearly everywhere on the dayside, instead of in the upper ionosphere. Their conclusions included inference of additional atmosphere escape due to greater exposure of the upper atmosphere oxygen and hydrogen exospheres to solar wind and magnetosheath-related ionization (by electron impact and charge exchange with solar wind protons), and planetary ion scavenging process. It is also worth noting that both the Phobos-2 and MGS missions occurred during the maxima of the two previous, relatively active solar cycles of the space age.

Mars Express carried instruments that significantly added to the availability of observations of solar wind interaction effects on Mars, with the Analyzer of Space Plasmas and Energetic Atoms IMA (ion mass analyzer) and MARSIS (Mars Advanced Radar for Ionospheric Sounding) providing insights on the space environment consequences. As MEX did not carry a magnetometer, the in situ analysis of the IMA ion mass spectrometer generally relied on assumptions regarding the field geometry based on MGS concepts of the solar wind interaction [e.g., *Brain et al.*, 2003, and references therein]. Using IMA data, *Edberg et al.* [2010] found statistical evidence that the measured planetary ion escape rates depended on the incident solar wind pressure, with average factors of ~2 enhancements in the escape rates for both solar wind stream interaction compression regions and passing ICMEs for the period studied. In addition, *Dubinin et al.* [2009] showed that faster, lower altitude energization of planetary pickup ions occurs when a solar wind enhancement goes by. Remote sensing by MARSIS provided both ionospheric electron densities and magnetic fields along the line of sight, giving independent information on the Mars deeper ionosphere responses to solar wind conditions. Detailed analyses using all available resources were carried out by *Opgenoorth et al.* [2013] for several interplanetary coronal mass ejection and solar wind stream interaction region-related events in March–April 2010, when conjunction geometry allowed use of near-Earth assets as upstream solar wind monitors, and by *Morgan et al.* [2014] for an ICME event in June 2011 when the suite of relevant MEX observations allowed a relatively close look at the ionospheric response(s). In agreement with *Crider et al.* [2005], these studies found apparent

compression of the Mars obstacle, with the observable ionosphere in the subsolar region diminished well below normal altitudes, even lower than the MEX periapsis at ~250 km. The presence of stronger than typical subsolar magnetic fields was also inferred from MARSIS results, and both MARSIS and in situ observations suggested that the ionosphere extends well past the terminator plane on the disturbed orbits. The presence of low-altitude magnetosheath electron fluxes and related enhanced penetration of solar wind proton fluxes would be expected to provide sources of additional ionization that could in part explain the postterminator ionosphere results, although enhanced transport from the dayside could not be ruled out.

From its inception, understanding Mars' solar wind interaction responses to space weather events has been part of the MAVEN mission's science goal of reconstructing the history of atmosphere loss to space [*Jakosky et al*., 2015b]. The mission's instrument complement, including plasma and energetic particle detectors, ion mass spectrometers, a solar EUV monitor, and magnetometer, was specifically targeted toward detecting space environment conditions and related changes in the Martian magnetosphere, ionosphere, and solar wind interaction. One aspect of a mission over which there is little control is the behavior of the Sun. Solar events are by their nature sporadic and directional, and as a rule, there are no guarantees concerning what numbers and types of events will occur at Mars over a specific time period. The unusually weak recent cycle has thus dictated what has been learned over the year-long MAVEN primary mission. The largest event observed up to the present, an ICME in March 2015, would be categorized as moderate by Earth-impact standards [see *Lee et al*., 2017]. It had peak plasma velocities of ~800 km/s, dynamic pressures of ~20 times the pre-event level, and maximum interplanetary magnetic field strengths of up to ~20 nT. This example allowed us to analyze Mars' global atmosphere escape response with the aid of global models of the solar wind interaction. [*Jakosky et al*., 2015a; *Curry et al*., 2015; *Dong et al*., 2015]. We revisit this event period to better understand some of the details of Mars' response in light of what is known about major ICMEs in general and from the models. We then use knowledge of the properties of a much more extreme event observed by the STEREO A spacecraft at 1 AU on 23 July 2012 [*Liu et al*., 2014]—together with the same data-validated simulation of the Mars-solar wind interaction—to infer the potential consequences compared to what we have observed. The results can be viewed as providing perspective for ongoing MAVEN investigations and for assessing the role of solar events as the Sun and solar system evolved.

2. Mars-Solar Wind Interaction and the Nature of ICMEs

Interplanetary coronal mass ejections, ICMEs, and the Earth's response to them have been studied for decades in the heliospheric science community [e.g., *Schwenn*, 2006]. They are widely understood to result from the eruption of solar coronal material, whose magnetic fields sometimes resemble large (approximately tenths of an astronomical unit) magnetic flux ropes when detected by in situ plasma and field instruments in the inner heliosphere [e.g., *Li et al*., 2014, and references therein]. While the typical solar wind plasma flows outward from the Sun at ~300–600 km/s, a few ICMEs emerge from the corona at speeds up to ~2500 km/s. The related ICMEs decelerate via interactions with the ambient medium but can still result in plasma moving at up to ~2000 km/s at 1 AU. The most extreme interplanetary conditions in the inner heliosphere are thus associated with ICMEs. These space environment disturbances include a leading shock wave in the solar wind at which the velocity, density, and temperature of the plowed-up ambient solar wind plasma can take significant jumps, followed by the strongly magnetized coronal ejecta that may extend the ICME duration for up to several days. SEPs related to the ICME shock can also have planetary consequences. Discussions of the relationship between ICME shocks and SEPs can be found in the *Aran et al*. [2007] and *McKenna-Lawlor et al*. [2005, and references therein]. It is also worth mentioning here that ICME disturbances may be further enhanced by interactions with ambient solar wind stream structures, including both solar wind stream interaction regions and other ICMEs [see *Lee et al*., 2017].

Earth's particular response to an ICME, the geomagnetic storm, is strongly controlled by its important internal dipole magnetic field, which produces the magnetosphere. A large body of work and related publications exist describing the detailed nature and consequences of geomagnetic storms [e.g., *Vennerstrom et al*., 2016, and references therein]. In particular, it has been realized since the 1960s [*Dungey*, 1968] that a parameter of major importance in an ICME's influences on the Earth or "geoeffectiveness" is the southward component of the out-of-ecliptic interplanetary magnetic field B_z. If the ICME produces (by virtue of the snowplowing compression of ambient solar wind field or by its internal coronal ejecta fields, or both) a

large and long-lived interval of southward B_z, a major storm will occur. In contrast, in the case of a northward or only weakly southward B_z ICME, the Earth responds mainly to the solar wind dynamic pressure enhancement. The physics of geomagnetic storms including the generation of the ring current, radiation belt enhancements, auroras, and related ionospheric disturbances have been studied for decades. At the most basic level these storms are understood to be the consequence of the combination of magnetospheric compression and magnetic reconnection of its field with the interplanetary magnetic field, allowing coupling of the solar wind convection electric field $E = -V \times B$ into the magnetosphere and the ionosphere at its inner boundary. Some effects of particular interest include radiation belt enhancements [e.g., *Shprits et al*., 2011], ionospheric disturbances [*Manucci et al*., 2005], and upper atmosphere ion energization and outflows [*Strangeway et al*., 2005; *Moore and Khazanov*, 2010]. Geomagnetic storm details continue to be investigated with improving mission designs, instruments, and sophisticated modeling, including simulations of the solar wind interaction with the magnetosphere coupled to the ionosphere at its base.

The Mars response to an ICME is expected to differ considerably from that of the Earth. First, the solar wind pressure balance with the Mars combined (ionospheric thermal pressure + crustal magnetic field pressure) obstacle is already marginal under normal conditions [e.g., *Zhang and Luhmann*, 1992; *Brain et al*., 2005]. The ability of fields from induced (Venus-like) ionospheric currents and the crustal fields to divert the oncoming magnetized incident plasma and field is expected to become even less effective as the shocked, piled-up solar wind and interplanetary field of the ICME sheath arrive, and as the following, longer duration strong field ejecta phase passes on timescales of up to days. Understanding the resulting transformation of the Mars plasma interaction and its consequences, the Mars analog of a geomagnetic storm, is the goal of the analyses described here.

3. Revisiting the March 2015 Event

The 6–8 March 2015 ICME event at Mars was described in the MAVEN First Results issue of Science by *Jakosky et al*. [2015a]. Those authors focused on the question of how much the atmospheric ion escape rate was affected by its passage. The use of the BATS-R-US global MHD simulations of the Mars-solar wind interaction [*Ma et al*., 2004; *Ma and Nagy*, 2007] to infer global implications of the local (orbital, in situ) measurements was also described. These models, developed before the MAVEN mission was realized, are described in the above-cited publications, and so we refer the interested reader to those for details—including the photochemical reaction rates used to produce the ionosphere in the models. For our purposes, a key attribute of the models is the ability to simulate the global system for virtually any user-specified external conditions (of solar EUV flux and incident plasma and magnetic field), with the caveat that assumptions concerning ionosphere production mechanisms and rates, and imposed boundary conditions at the ~100 km inner boundary altitude of the model, are held fixed. The basic agreement of orbit samples of three steady state multispecies single fluid models with observations of the plasmas and magnetic field along the MAVEN orbit during the March 2015 event, as well as under quiet conditions [*Ma et al*., 2015], gave confidence in the inferred global ion escape rate enhancements. While both time-dependent [*Ma et al*., 2017] and multifluid [*Dong et al*., 2015] versions of these models exist, the steady state snapshot approach may be appropriate for ICMEs because they include periods when conditions change slowly compared to the solar wind interaction response timescale. Exceptions occur during rapid/narrow transition periods like the leading shock passage, the ICME sheath/ejecta interface, or occasional heliospheric current sheet crossings that are sometimes integrated into the magnetic topology of ICMEs.

The successful March 2015 event model time series comparisons raise the question of what is happening in the Mars magnetosphere and ionosphere on a more global scale during this time. At the Earth, a magnetic storm has phases corresponding to the passing ICME structure. In the March 2015 event model application, three steady state snapshots of the solar wind interaction essentially sample the system before the ICME arrives, during the compression associated with the high dynamic pressure in the shocked ICME sheath plasma and then in the strong field ICME ejecta. In a manner analogous to applications of Earth magnetosphere-solar wind interaction simulations, we use the model results to investigate these questions: How does the Martian magnetosphere magnetic field topology change during the event? What does this imply for direct solar wind and solar particle access to Mars' atmosphere? What are the consequences for the ionospheric dynamics and outflows?

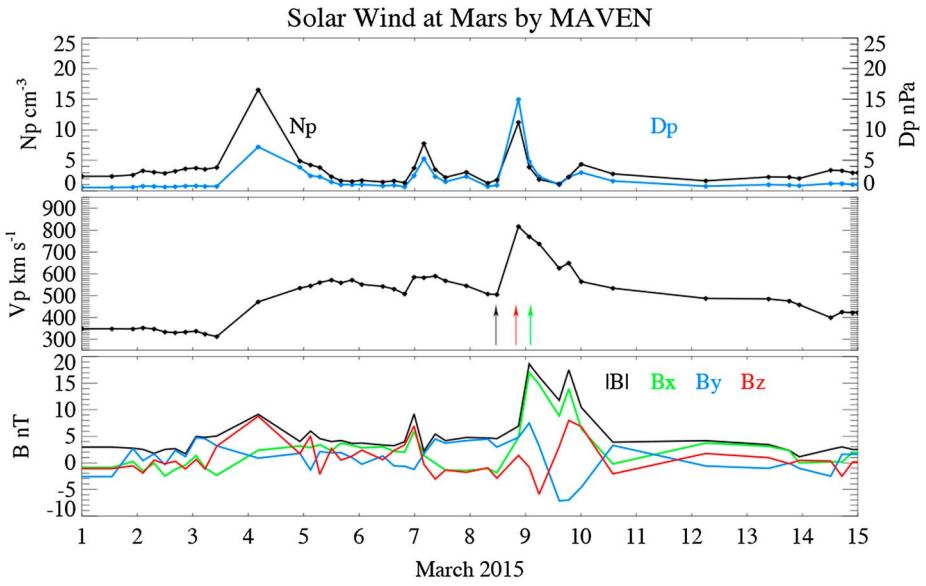

Figure 1. Time series of solar wind plasma and magnetic field measurements obtained by the MAVEN SWIA and the magnetometer, showing the largest ICME event detected during the prime mission and its context in the surrounding weeks. Arrows show times used for model upstream parameters: preICME (black), ICME sheath (red), ICME ejecta (green).

Figure 1 shows the external conditions surrounding the March 2015 MAVEN ICME event as observed with the combination of the solar wind ion analyzer (SWIA) solar wind plasma analyzer [*Halekas et al*., 2013] and magnetometer [*Connerney et al*., 2015]. The coordinate system used for the magnetic field vector components is the standard mars solar orbital (MSO) Cartesian system where x is the Mars-Sun axis, y is in the direction opposite Mars' orbital motion, and z is northward out of the Mars orbit plane. The times selected for the three simulations for this event are marked with small arrows (also see *Jakosky et al*. [2015a, Figure 2]). For context, it is worth mentioning that solar wind plasma velocities at Mars are expected to have essentially the same range of values (~300 km/s to ~600 km/s) as at the Earth [e.g., *Opitz et al*., 2010], while densities are on average reduced by $1/(1.5)^2$ to account for Mars greater distance from the Sun. The average interplanetary magnetic field radial component is similarly expected to be reduced by r^{-2}, while the perpendicular (to the flow) component, which is normally close to the Mars orbital plane, is reduced by r^{-1} according to standard Parker Spiral interplanetary field geometry assumptions—though the latter does not necessarily apply during an ICME. Table 1 shows the upstream parameters used for the three MHD simulations for this event, the same information as provided by *Curry et al*. [2015]. As the simulated time series comparisons of the model results with both the in situ solar wind and planetary ions, and magnetic field measurements on MAVEN are shown by these authors, we do not repeat them here, instead proceeding to their implications.

Figure 2 shows two views (noon-midnight meridian and solar viewpoint projections) of the model magnetospheric field topology for the three March 2015 ICME phases. These field line tracings are started on a dense grid of points on a spherical surface at 150 km altitude, the nominal periapsis altitude of MAVEN. They are color coded according to whether the tracing leads to both ends of the field line at the inner boundary of the model at 100 km—the closed field lines (red), one end at the inner boundary and one end exiting a spherical surface at 4 R_m—the open field lines (green), or both ends ending on this outer surface—and the draped field lines (blue). As seen in Figures 2a and 2b, for the pre-ICME (case 1) model snapshot the magnetic fields at 150 km on the dayside are largely closed, although the meridian view shows that somewhat irregularly shaped "polar caps" of open field lines exist. These extend into tail lobes like a weak intrinsic magnetosphere, sandwiching stretched, dipole-like closed field lines in between. There is no contribution of draped field lines to this picture, which generally appear in greater numbers when higher altitude starting points are used [e.g., see *Luhmann et al*., 2015a]. The ICME sheath phase topology in Figures 2c and 2d (case 2) features the greater occurrence of open field lines on the dayside. The meridian view also shows this greater incursion of open field lines, the result of the enhanced dynamic pressure and enhanced reconnection of the draped

Table 1. Parameters Used for the March 2015 MAVEN ICME Case

8–9 March 2015 Case[a]	N_{sw} (cm^{-3})	V_{sw} (km/s)	B_{imf} (nT)	Global Escape Rate (s^{-1}) (O^+, O_2^+, CO_2^+ Total)
preICME	1.8	(−505, 15, −10)[c]	(−2.5, 2.8, −3.0)[c]	2.0×10^{24}
ICME sheath	11[b]	(−815, 60, 0)[d,c]	(5.2, 5.4, 1.7)[c]	1.7×10^{25}
ICME ejecta	4.5	(−780, −45, −10)[c]	(19.1, 7.6, −0.8)[e,c]	1.0×10^{25}

[a]Parameters from *Curry et al.* [2015].
[b]Peak density.
[c]MSO coordinates.
[d]Peak speed.
[e]Peak B and B_x dominates.

interplanetary fields with the crustal fields. The hemispherically unequal distribution of the new open field regions at 150 km, with more open lines in the northern hemisphere, suggesting that the stronger southern hemisphere fields are deflecting more of the locally incident solar wind flows, still providing effective shielding for that portion of the Mars obstacle. In the last case, the ejecta phase (case 3), the magnetic fields are still strong but the incident solar wind pressure is not so enhanced due to reduced density (Table 1). However, what is striking about this period is the large B_x component. In classic, direct ICME impacts seen at 1 AU, the dominant ICME ejecta fields are often perpendicular to the incident solar wind flow. This is because the strongest field is near the flux rope axis which lies near the MSO equivalent *y-z* plane in a direct hit. A large *x* component of the field as seen in this case might be attributed to intersection with one of a flux rope's solar-attached legs [e.g., *Neugebauer et al*., 1997]. Thus, the March 2015 MAVEN ICME ejecta are not so ideal. This topology is reflected in the model field lines in Figures 2e and 2f. The fields at 150 km are more open overall, consistent with increased reconnection with the strong external field, even with the atypical external orientation. But the open fields are more hemispherically symmetric than in the preceding sheath phase, in part because the strong crustal fields have rotated into the wake where they have less influence on the dayside solar wind interaction. This more *x*-directed orientation of the ejecta fields also has potential consequences for the effects of this phase of the March 2015 event in that the $E = -V \times B$ solar wind convection electric field is reduced from its maximum possible value when V and B are more nearly parallel.

The locations of the plasma interaction boundaries (the bow shock and magnetic pileup region) described in the literature on this event are consistent with previously reported observations of dayside obstacle compression and solar wind access to lower than typical altitudes during solar wind pressure enhancements [e.g., *Brain et al*., 2005; *Crider et al*., 2005; *Opgenoorth et al*., 2013]. But these models allow visualization of the related planetary ion redistribution and escape, as determined by MHD forces (e.g., pressure gradient and $J \times B$). Table 1 also includes the combined escape rates of the model planetary ion species ($N_i = O^+$, O_2^+, and C O_2^+) for the March event. The spatial distributions of the total heavy planetary ion densities and fluxes for the three phases of the event are shown in Figures 3 and 4 for the noon-midnight meridian planes. Complementary plots of the normalized (by the scalar quantity) magnetic and velocity vectors in the meridian plane are included in Figure 5. These results can be compared to the averaged, observation-based planetary ion flux maps described by *Brain et al*. [2015] because they suggest complicated structures of outflows exist even for global snapshots. In particular, the classical and often-used induced magnetotail heavy ion plasma sheet picture does not, in general, apply in the vicinity of Mars [see *Luhmann et al*., 2015b]. The vector plots in Figure 5 also suggest a complicated relationship exists between the planetary ion flows and fields. In addition, these pictures are snapshots of a quasi-steady numerical simulation, which from time step to time step exhibits changes in details. The numerical diffusion-controlled reconnection process in even quasi-steady simulations is inherently bursty, although the general mesoscale structure of the interaction is maintained [*Fang et al*., 2013]. In addition, these models neglect additional time dependence from the rotation of the crustal magnetic fields with the planet [*Ma et al*., 2014]. Thus, in spite of their complexities, the model results described here must be regarded as having a number of simplifying approximations and limitations.

The magnetic topologies in Figure 2 have implications for related energy and particle exchanges between the upper atmosphere of Mars and the surrounding space. Figure 6 shows day and nightside views of areas on a 150 km surface, near the MAVEN periapsis, where the model fields are open (green), closed (red), or draped (blue) topologies. These give an idea of where solar wind and solar suprathermal electrons have

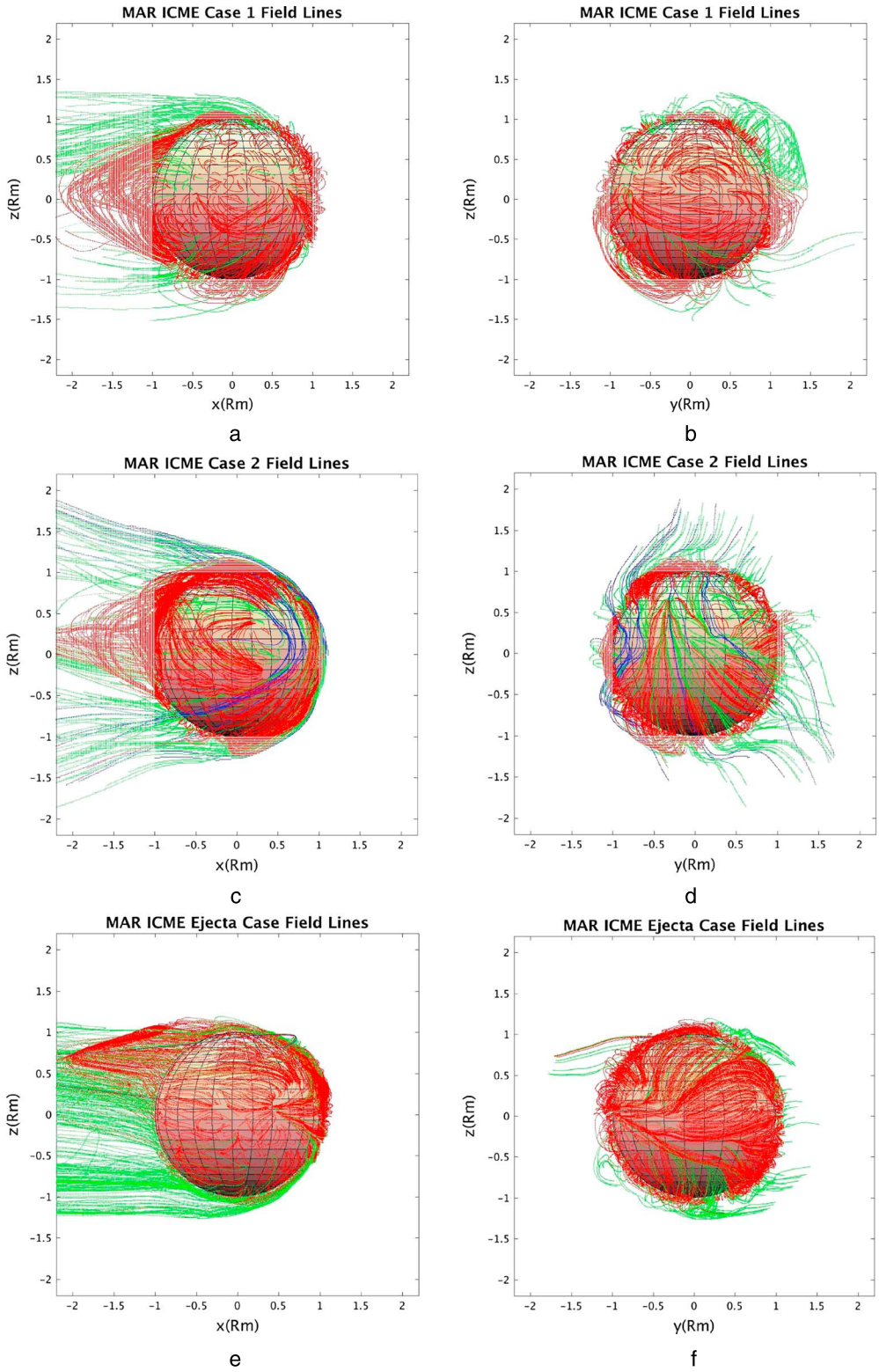

Figure 2. Projections of 3-D model field lines for the (a and b) noon-midnight meridian and (c–f) as viewed from the Sun for the three models run for the March 2015 MAVEN ICME event passage [*Jakosky et al.*, 2015a]. The Mars surface is represented by the shaded globe in the center of this planet centered (MSO) coordinate system. All field lines shown, which are the same field lines in both views of each case, are traced from a starting grid at 150 km altitude. Red identifies closed field lines, green is used for open fields, and blue (not seen in these cases) for draped field lines. The times marking the upstream conditions for the models are marked in Figure 1, with the leftmost plots the pre-event case and time increasing left to right.

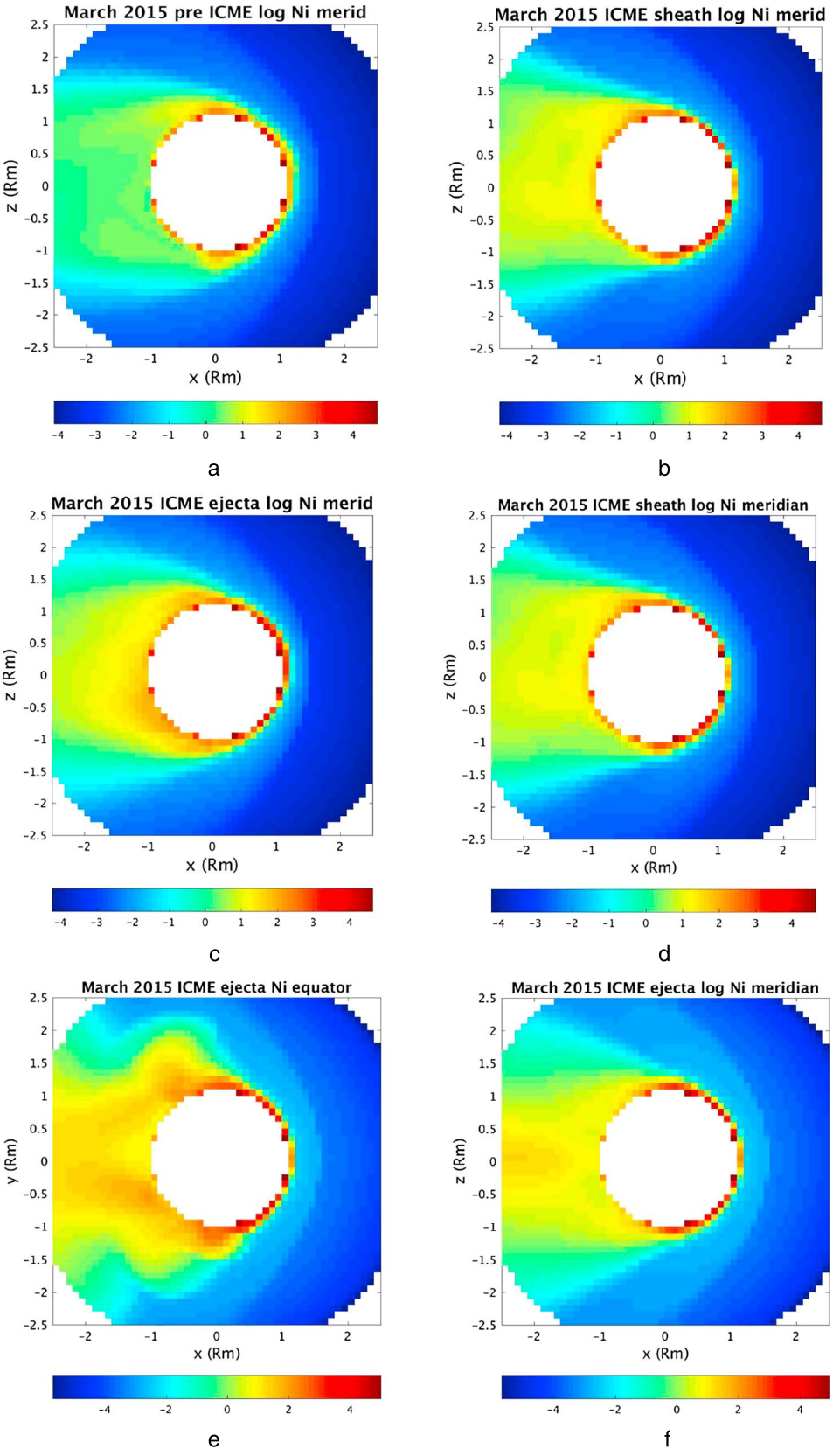

Figure 3. Meridian plane slices of the model ionospheric densities (log (cm^{-3}) scale) for the three March 2015 event model cases with time increasing left to right.

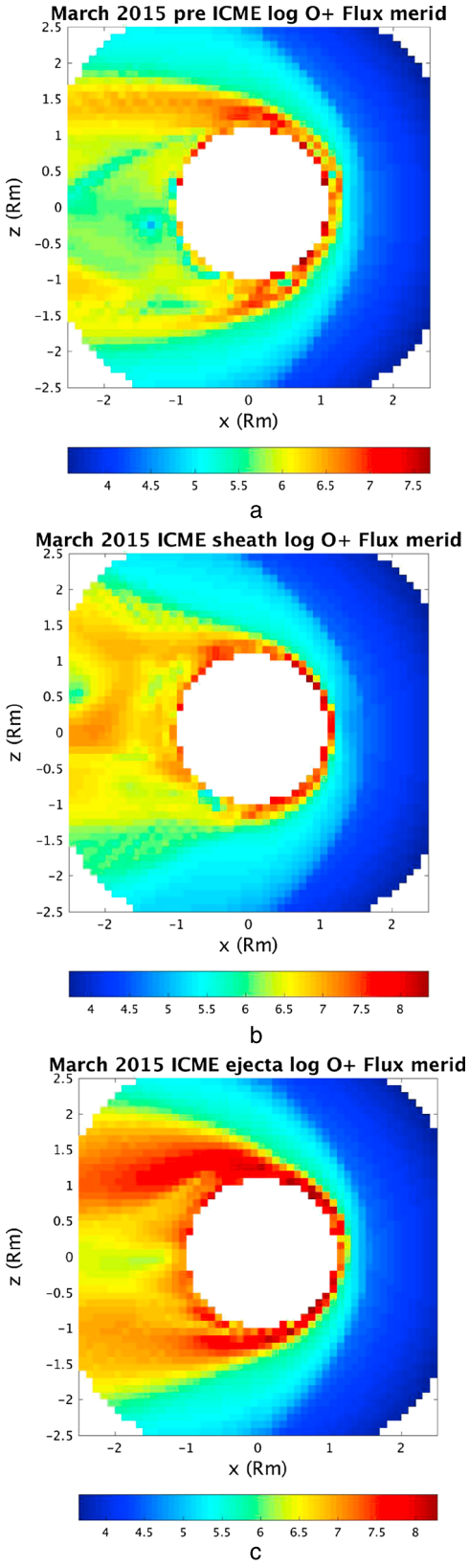

Figure 4. Meridian plane contours of ionospheric ion (log (cm^{-3} s^{-1})) fluxes for the March 2015 event cases with time increasing left to right, for comparisons to their density counterparts in Figure 3.

relatively direct access to the atmosphere. This has implications for both the importance of ionospheric production by electron impact ionization and also for the spatial distribution of the nightside diffuse auroral emissions reported by MAVEN Imaging Ultraviolet Spectrograph investigators. The diffuse UV auroras were found to be associated with energetic electrons from solar events—including the March 2015 ICME [*Schneider et al.*, 2015]. Although global UV aurora snapshots are not possible with the existing instrumentation, the diffuse aurora and energetic solar electron relationship has been clearly established. The patchy patterns of the open fields in Figure 6 [see also *Ulusen et al.*, 2016] result from the particular combination of external parameters and crustal field locations that prevail in each case. In particular, interplanetary field orientation will determine where the crustal and draped interplanetary fields are more nearly antiparallel, leading to efficient magnetic merging of the two, while the incident solar wind pressure determines the depth to which such merging can occur. As the event progresses, the area of open and draped fields (green and blue points in Figure 6, respectively) at this low altitude increases from the pre-ICME phase to the sheath phase to the ejecta phase, with the latter the most "open" field geometry for this event. Although most of the increases of the open field areas are on the dayside, this can still affect what is observed on the nightside, for example, the occurrence of photoelectrons in the solar wind wake [e.g., *Liemohn et al.*, 2006]. And as already alluded to above, the amount of open field affects the extent to which solar wind convection electric fields map into the coupled magnetosphere-ionosphere system.

The effects on low-altitude magnetic fields, ion velocities, and densities in the solar wind/obstacle boundary

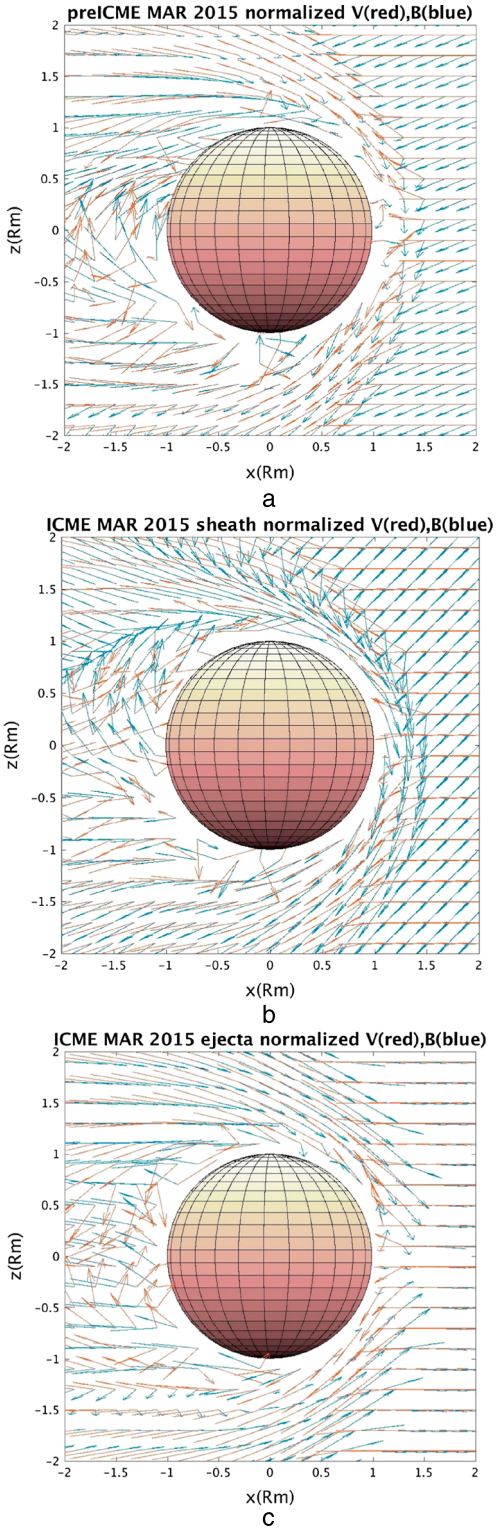

Figure 5. The meridian projections of the normalized velocity (red) and magnetic field (blue) vectors for the March 2015 event models for comparison with the ionospheric ion fluxes in Figure 4. Normalization involves dividing by the scalar value, so these are unit vectors. Again, time increases from left to right. Notice the relative orientations of the field and velocity vectors in the right panel suggest polar wind-like outflows from high latitudes during the ejecta phase.

region and at exobase altitudes (nominally below ~200 km) are also of interest. Figures 7 and 8 show MSO latitude/longitude maps of the radial (vertical) components of the magnetic field B_r, plasma velocity V_r, and planetary heavy ion density N_i at the nominal 400 km altitude of MGS and the 150 km periapsis altitude of MAVEN for the three modeled phases of the March 2015 event. The midnight meridian is located at the centers of these maps at 180° "longitude." The vertical velocity component is shown because it is normally negligible at these altitudes, and thus, perturbations stand out. The influence of the high dynamic pressure ICME sheath phase is most apparent in the 400 km maps in Figure 7. The modeled V_r changes are patchy and mostly positive (outward). The heavy ion density maps for this altitude also show increases reflecting the greater compression of the ionospheric plasma at this altitude, although the upward vertical velocities should also bring more ionospheric plasma into this region from below. Ionosphere upwelling due to penetrating convection electric fields has also been reported during geomagnetic storms [e.g., *Manucci et al.*, 2005] although the penetration and upwelling details are quite different in that the geometry is heavily controlled by Earth's dipole field. A mixture of patchy upwelling and downward flows also occurs during the ejecta phase simulation, but to a lesser extent. The analogous situation at 150 km (Figure 8) shows weak downward velocities during the event, but the density map differences are most noticeable, with the nightside ionosphere essentially absent during the pre-ICME phase, and an excess of nightside density in the northern hemisphere for the sheath and ejecta phase maps. A consideration here is that the strong crustal fields, seen in the B_r maps, rotated into the midnight

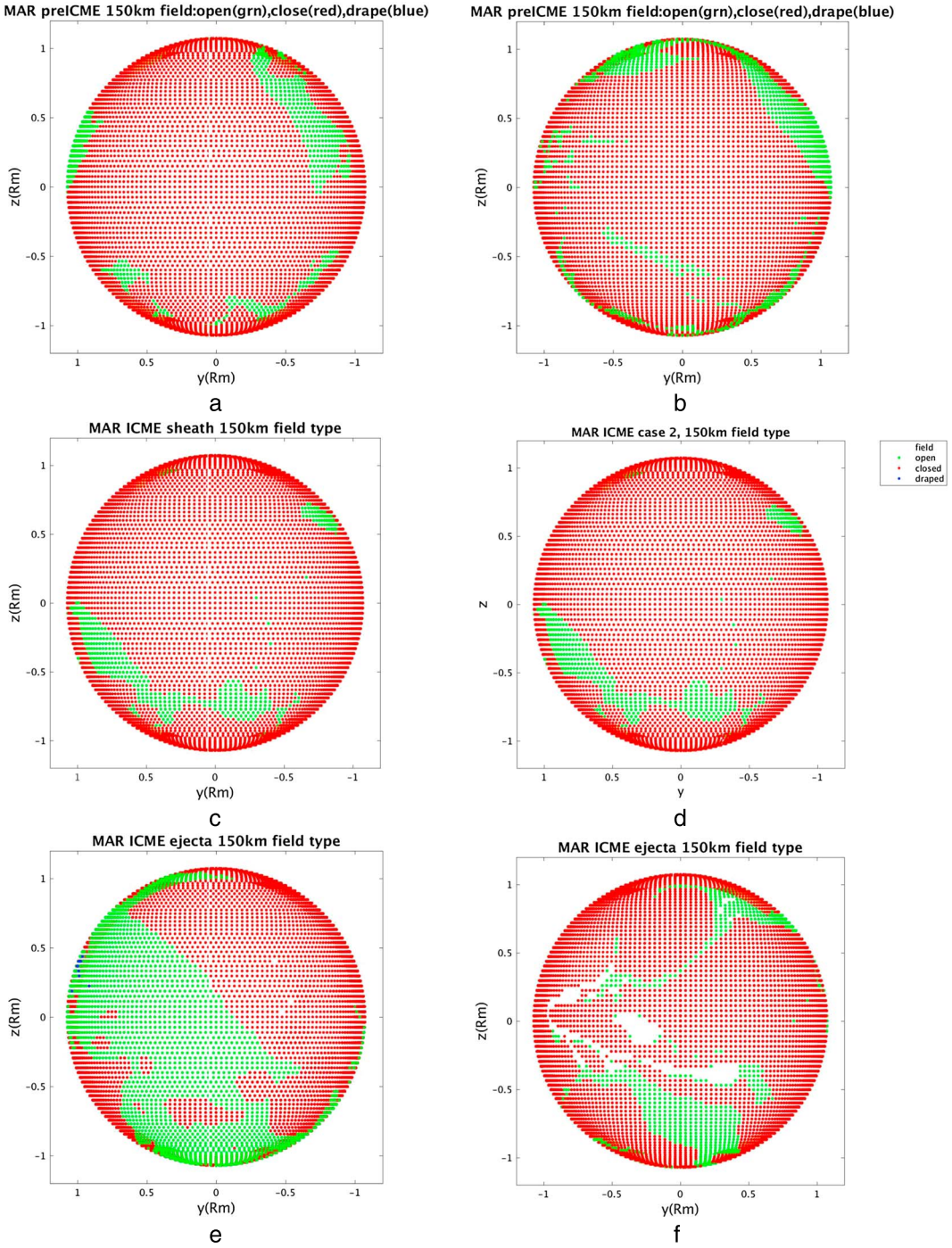

Figure 6. (a and b) Nightside and (e and f) dayside full-disk views of the magnetically closed (red), open (green), and draped (blue) field starting points at 150 km of the field lines show in Figure 2 for the March 2015 ICME event model cases. Time increases left to right. The green and blue areas represent locations where external/interplanetary electrons can have relatively direct access to this altitude, possibly initiating diffuse auroras and their associated nightside ionization. White areas in Figure 6f correspond to field line tracings from 150 km that follow routes not intersecting neither the inner nor outer boundary—often appearing like closed loops.

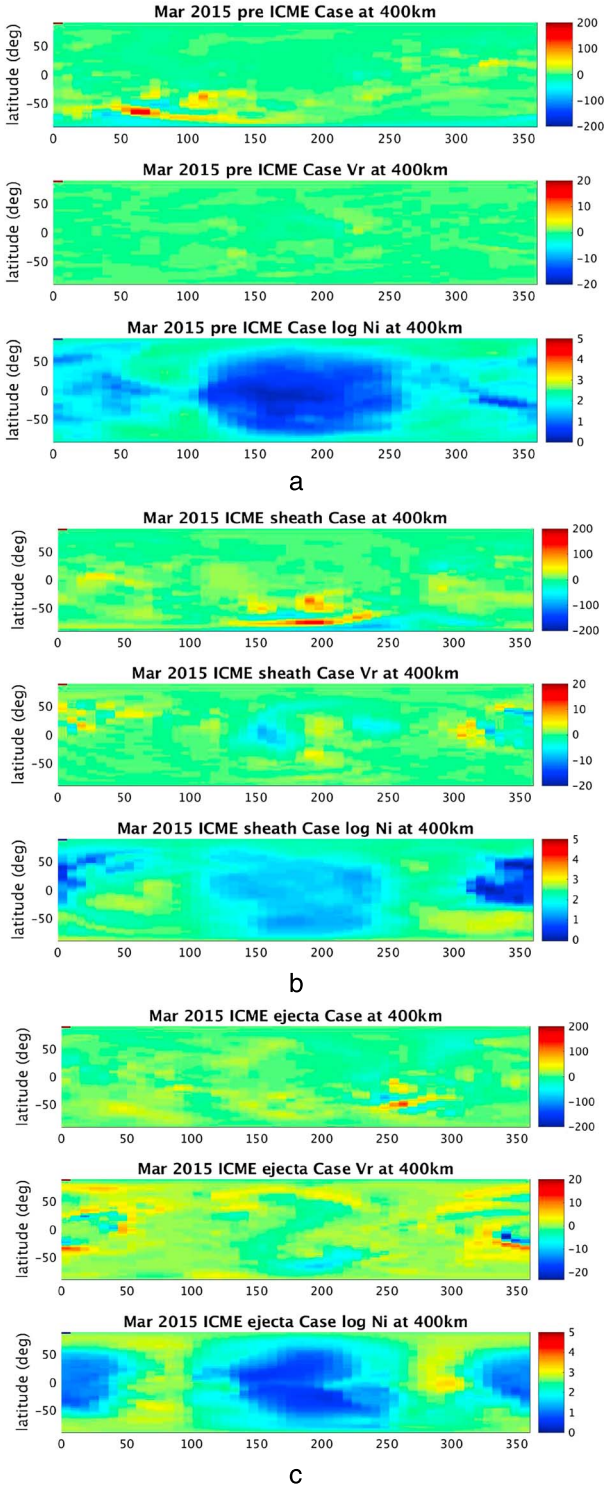

Figure 7. Maps of selected March 2015 event model parameters at 400 km in the MSO system where longitude represents local time (180° is the midnight meridian here). The values chosen for the color contours here are the radial field with respect to Mars (B_r) (units in nT), the vertical plasma velocity V_r (in km/s), and (log) planetary ion density N_i. The time sequence of the models again runs left to right. Changes are caused by the ICME event in all parameters at this altitude including local enhancement of ionospheric ions and usually small vertical velocities.

sector, probably preventing access to ionospheric ions transported from the dayside that seem to populate the northern nightside. One question of course is whether these behaviors are observed, and whether they represent behavior specific to the March 2015 event conditions.

4. An Extreme Event Experiment

The inferred enhancements to Mars magnetosphere-solar wind coupling that the March 2015 ICME event produced raise the question of how extreme such interactions can become. In section 1 several record-making (by present day standards) events that occurred while Phobos-2 and MGS were at Mars were described. However, the limitations of the available measurements were also noted. In their study of several moderate solar event effects with MEX, *Opgenoorth et al.* [2013] adopted the upstream monitor approach to aid in interpreting the observations by choosing a period when conjunction allowed Earth upstream solar wind monitors to be used. They applied standard interplanetary plasma and field transport assumptions to the ~1 AU measurements to describe the Mars external environment associated with both ICME and solar wind stream interaction disturbances detected in the MEX plasma and ionospheric radar data. Although Mars and Earth locations were similarly advantageous, this method could not be used for the MGS extreme events in October–November 2003 because the near-Earth measurements have significant data gaps at critical times. Indeed, it is often the case that out-of-nominal-instrument-range values of the plasma parameters compromise extreme event observations. Given these circumstances, numerical experiments provide an alternative means of investigation, especially in view of the good performance of the

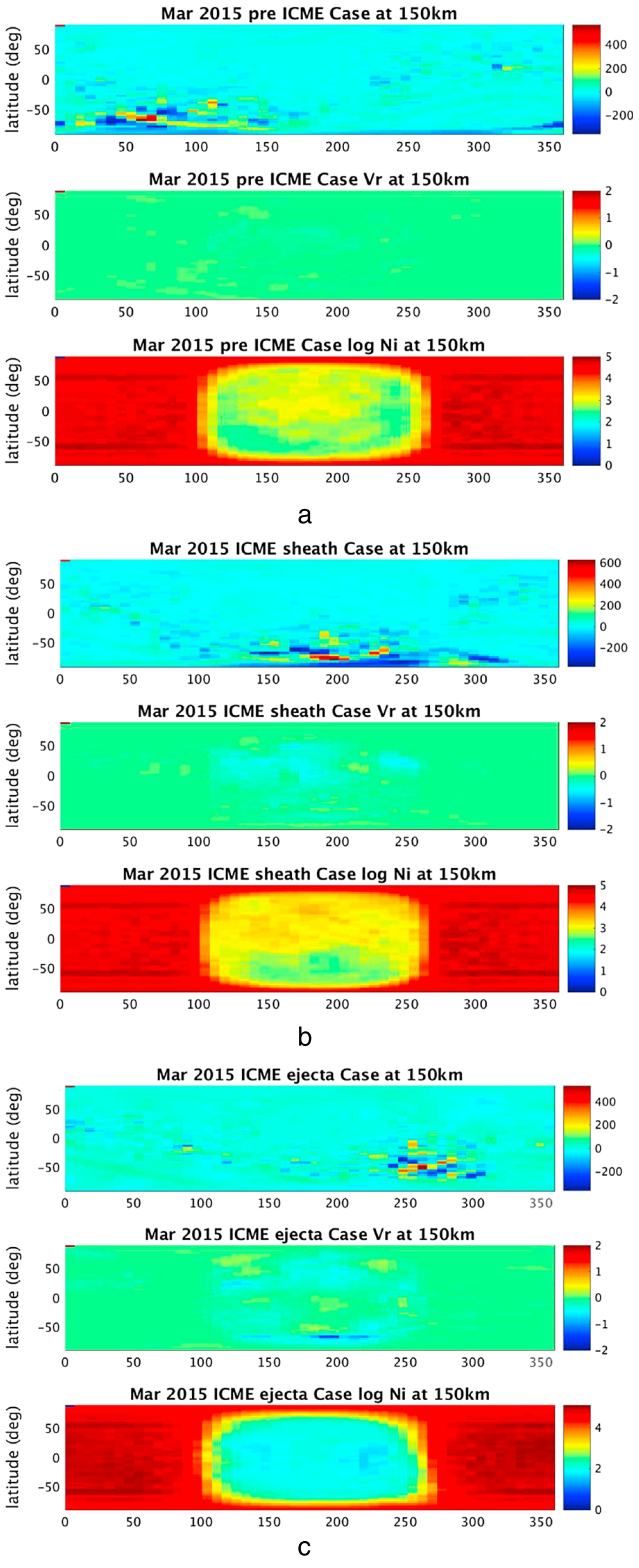

Figure 8. Same as Figure 7 but for 150 km altitude. (b, bottom) The appearance of enhanced model planetary ion fluxes in the nighttime northern hemisphere and (c, bottom) the apparent reduction in ionospheric ion density at night during the ejecta phase suggest the effects of the March 2015 ICME event, in spite of its moderate strength, can have deep impacts.

solar wind interaction models applied to the March 2015 event.

Arguably the most complete interplanetary data set related to what is widely acknowledged as one of the most extreme events on record is from a 23 July 2012 solar eruption that produced an ICME event detected within a day at 1 AU on STEREO A [e.g., see *Liu et al.*, 2014]. Figure 9 shows the 1 AU ICME plasma and field parameters from Liu et al., including portions where special methods had to be employed to derive the plasma speeds and densities. The parameters in this event can be compared with those shown in Figure 1 for the March event. The peak velocity is several times higher, which translates to an even larger dynamic pressure enhancement. Even with the application of nominal r^{-2} radial decreases in both the plasma density and radial (x) magnetic field components, and a nominal r^{-1} applied to the perpendicular magnetic fields, this event would have been exceptional at Mars. Though this ICME missed both Earth and Mars due to their large angular separations from STEREO A at the time (the responsible coronal mass ejection was centered on STEREO A, on the opposite side of the Sun from Mars), both locations were exposed to some of the solar energetic particles generated at the strong ICME shock. We take advantage of the availability of these measurements from an observed extreme ICME and the BATS-R-US Mars-solar wind interaction model to investigate what its effects at Mars might have been.

Table 2 contains upstream parameters for three model cases run for this hypothetical extreme ICME event, where the values are based on pre-event conditions, the ICME sheath interval, and a sample from the ejecta phase, as identified in Figure 9. These parameters were extrapolated to Mars orbit using the scalings described above, assuming

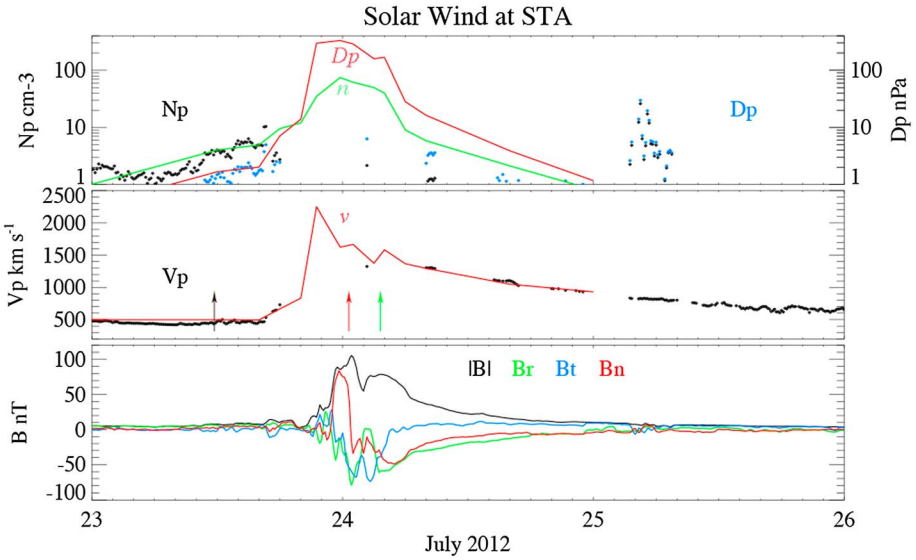

Figure 9. Time series analogous to Figure 1 of the extreme event observed on STEREO A at 1 AU in July 2012. This is one of the largest and strongest ICMEs on record for which a fairly complete record of the interplanetary plasma and field data is available. The lines that bridge the data gaps, as noted in the text, required special procedures as described in *Liu et al.* [2014]. Times chosen for model experiments with Mars distance extrapolations of parameters are indicated with arrows (black—preICME case, red—ICME sheath case, and green—ICME ejecta case).

no important deceleration or field reconfigurations occurred in the 0.5 AU between the planets. The resulting runs of the model ICME phases have magnetic fields up to ~60 nT compared to the ~20 nT maximum fields of the March 2015 case, maximum plasma density of ~25 cm^{-3} compared to ~10 cm^{-3} for March 2015, and velocities up to 1700 km/s compared to ~800 km/s. This extreme event is thought to have involved multiple material injections at the Sun, propagating into a rarefaction region produced by an earlier ICME passage [see *Liu et al.*, 2014]. As a result, there are larger than usual nonradial solar wind velocity components in the preICME case that create a noticeable deflection of the overall plasma interaction away from the usual MSO *x* axis. Moreover, the plasma speeds and densities during the most extreme part of the event had to be derived indirectly from some heavy ion measurements, in a manner which does not provide details on the velocity deflections during the event. Lastly, because the ejecta phase is affected by closely timed and spaced multiple injections at the Sun, it is not typical that the density (and dynamic pressure) remain significantly higher than the preICME value throughout. This history can affect the overall impact of such an event on the Martian system by prolonging the high incident dynamic pressures.

The results of the three simulation cases in Table 2, based on the July 2012 STEREO A event, are presented here in the same formats as for the March 2015 event. First, the global magnetic topologies are illustrated in Figure 10 in meridian and solar perspectives. Two features stand out in these pictures. First, the ICME sheath phase (Figures 10c and 10d) is dominated on the outside by draped magnetic fields. Recall that the field line tracings in these plots are all started on a spherical grid of points located at 150 km altitude. Thus, the magnetosheath/interplanetary fields have penetrated to these altitudes in this simulation, a result of the combination of extreme solar wind dynamic pressure forcing the pressure balance boundaries downward, together with downward diffusion of the strong, piled-up magnetosheath field. The ejecta phase field lines suggest that a majority of the 150 km surface (and where it maps to below) is open to the solar wind and connected to the interplanetary field.

Table 2. Model Parameters for the STEREO A July 2012 Extreme Event Extrapolated to Mars' Heliocentric Distance Using the Scaling Described in the Text[a]

Hypothetical STEREO A July 2012 Case at Mars	N_{sw} (cm^{-3})	V_{sw} (km/s)	B_{imf} (nT)	Global Escape Rate (s^{-1})
preICME	0.8	(−479, −44, −21)	(−2.3, 0.4, 1.1)	3.9×10^{24}
ICME sheath	24.8	(−1700, 0, 0)	(11.1, 6.7, 53.3)	1.4×10^{27}
ICME ejecta	4.4	(−1500, 0, 0)	(22.2, 20.0,−33.3)	6.1×10^{25}

[a]Solar maximum EUV conditions were used in these runs.

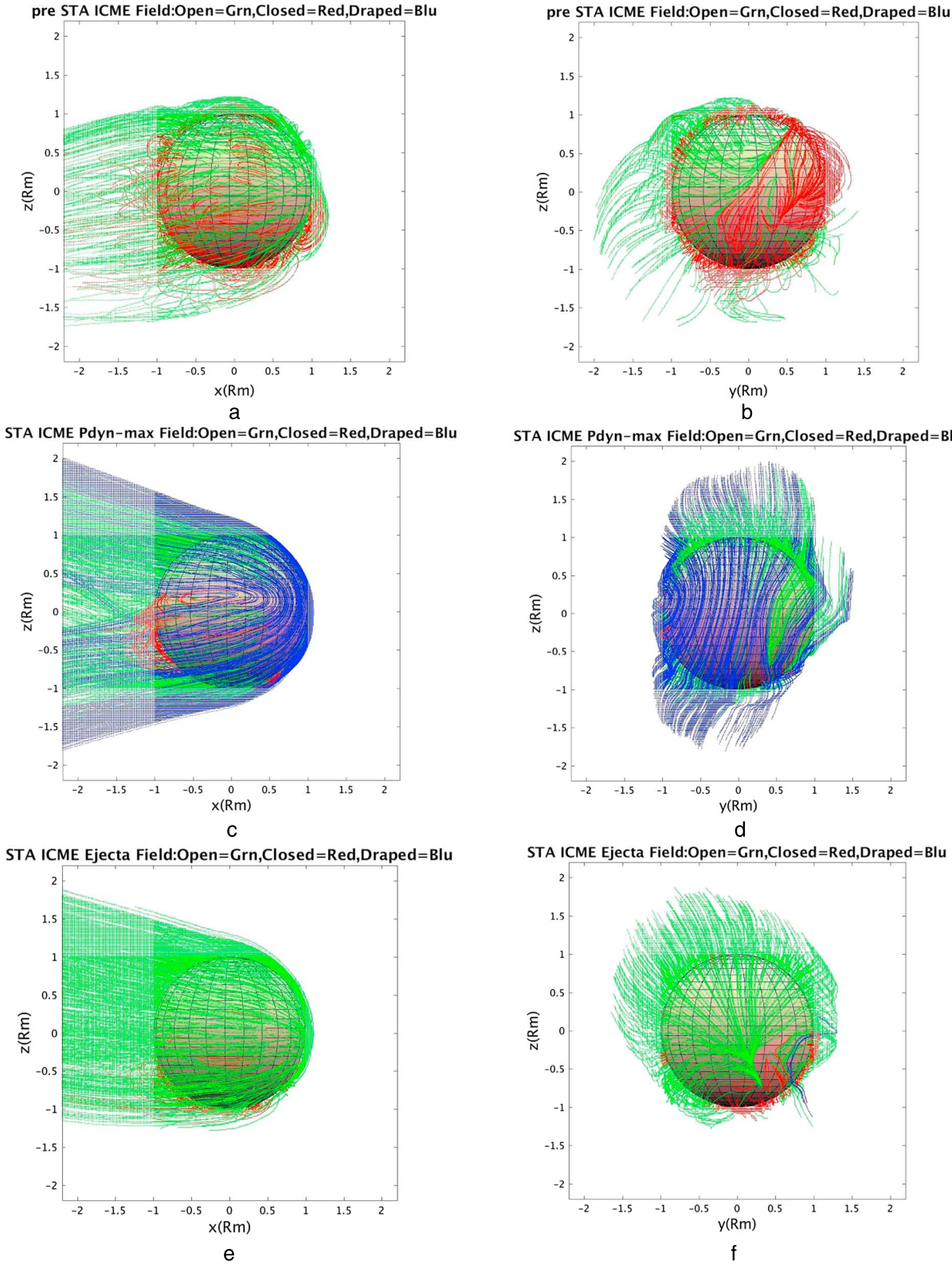

Figure 10. Same as Figure 2 but for the Mars distance extrapolated conditions of the July 2012 STEREO A extreme event (three phases: preICME, ICME sheath, and ejecta upstream conditions described in Table 2). Meridian and solar perspective projections of 3-D field lines traced from a 150 km grid. Red, closed fields; green, open fields; blue, draped fields. The appearance of many blue field lines in the center panels for the ICME sheath phase model is an important contrast to its March 2015 counterpart.

The patterns of the planetary heavy ion densities, and the fluxes and flows for this event, the counterparts of Figures 3–5 for the March 2015 event, are shown in Figures 11–13. Of main interest here are the particularly large fluxes during the ICME sheath phase (Figure 12b) and velocity vectors (Figure 13) indicating outward flows from low altitudes. The modeled sheath phase also dominated for the March 2015 event escape fluxes (Table 1). *Edberg et al*. [2010] already pointed out that dynamic pressure increases appear to be the primary drivers of increases in planetary ion escape as seen in MEX measurements and that this control holds over a range of dynamic pressure enhancements. Whereas the pre-event global ion escape rates in Table 2, obtained at the simulation outer boundary, were comparable to those found for the March 2015 event, the rate for the extreme event sheath phase is ~300 times larger—compared to ~10 times higher for the March 2015 sheath case. This much greater escape rate is consistent with expectations given the much lower altitude dayside penetration of the draped magnetosheath fields, and the much more open Mars magnetospheric topology indicated in Figure 10. The models include a combination of photoionization, electron impact ionization, and charge exchange with solar wind protons, the latter two of which are affected by the degree to which the ram face solar wind boundary is lowered, as well as the ability of external particles to access more of the atmosphere along open or even draped field lines.

Figure 14 shows the corresponding areas on the model dayside and nightside 150 km surface where the field lines are open, closed, or draped, as displayed in Figure 6 for the March 2015 case. The striking openness of the Martian "magnetosphere" for both the sheath and ejecta phases of this event is apparent, as well as the draped sheath field dominating the 150 km level over the dayside. According to these results, had this event occurred during MAVEN's prime mission and had periapsis been on the dayside, MAVEN would never have left the draped field region during the ICME sheath passage. Had periapsis been at night, sheath and SEP electrons (the latter of which were present at high fluxes throughout this event—see *Lee et al*., 2017) would have dominated throughout.

In addition to ion production considerations, the MHD forces working to expel the planetary ions are deeply and strongly engaged during this extreme event. In this context it is worth considering the Earth's magnetosphere for southward interplanetary magnetic fields and high incident solar wind pressure. For these favored magnetic storm conditions, the Earth's magnetosphere is similarly in its most magnetically open state. The terrestrial magnetic field connects through the magnetosheath to the interplanetary field within expanded high-latitude oval areas. Solar wind convection electric fields are imposed at thermospheric levels where they drive ionospheric convection in an ideally double-celled pattern where the flow is antisunward across the central polar cap, with return flows along the polar cap boundary. In the case of Mars during this extreme event, there is analogous widespread mapping to the upper atmosphere along open fields in the ICME sheath and ejecta phases (Figures 14c and 14d and 14b, 14d, and 14f). In other words, the implied upper atmosphere engagement is relatively global, with virtually no region of Mars—at thermospheric levels—left unexposed.

The final model diagnostic for this experiment is the global ionosphere maps in Figures 15 and 16, at 400 km and 150 km altitudes, showing vertical magnetic field, vertical velocity, and planetary heavy ion density for the three phases. The map sets for the two ICME phases suggest the extent to which the model ionosphere is altered by the extreme external conditions. The maps at 400 km exhibit large, patchy areas of strongly enhanced parameters. Strong noncrustal vertical fields in the center of the sheath phase map have the appearance of a double-lobed magnetotail with outward/antisunward field in the north and inward/sunward field in the south, reflecting the draped. Penetrated sheath field's high inclination (see Figure 10). The vertical velocity appears chaotic with upward and downward flows that in some spots reach the ~5 km/s escape speed for Mars. The ion density shows two low-latitude, cross-terminator enhancements associated with the highly inclined, sharply draped, penetrated field—akin to the roots of a Venus-like induced magnetotail with a planetary ion plasma sheet. The ICME ejecta counterparts (third set) also show patchy areas of high vertical velocities, though lower than for the sheath phase. A reminder here is that the simulation of this event is relatively dynamic, even though the external conditions in the simulations are steady. As in similar simulations for the Earth's magnetosphere interaction for southward interplanetary field, reconnections between the interplanetary and crustal fields modulate the associated wake ion outflows in a bursty manner. The results shown for the ion flows and fluxes represent snapshots of an interaction whose general, larger-scale features are maintained, but whose details change with time.

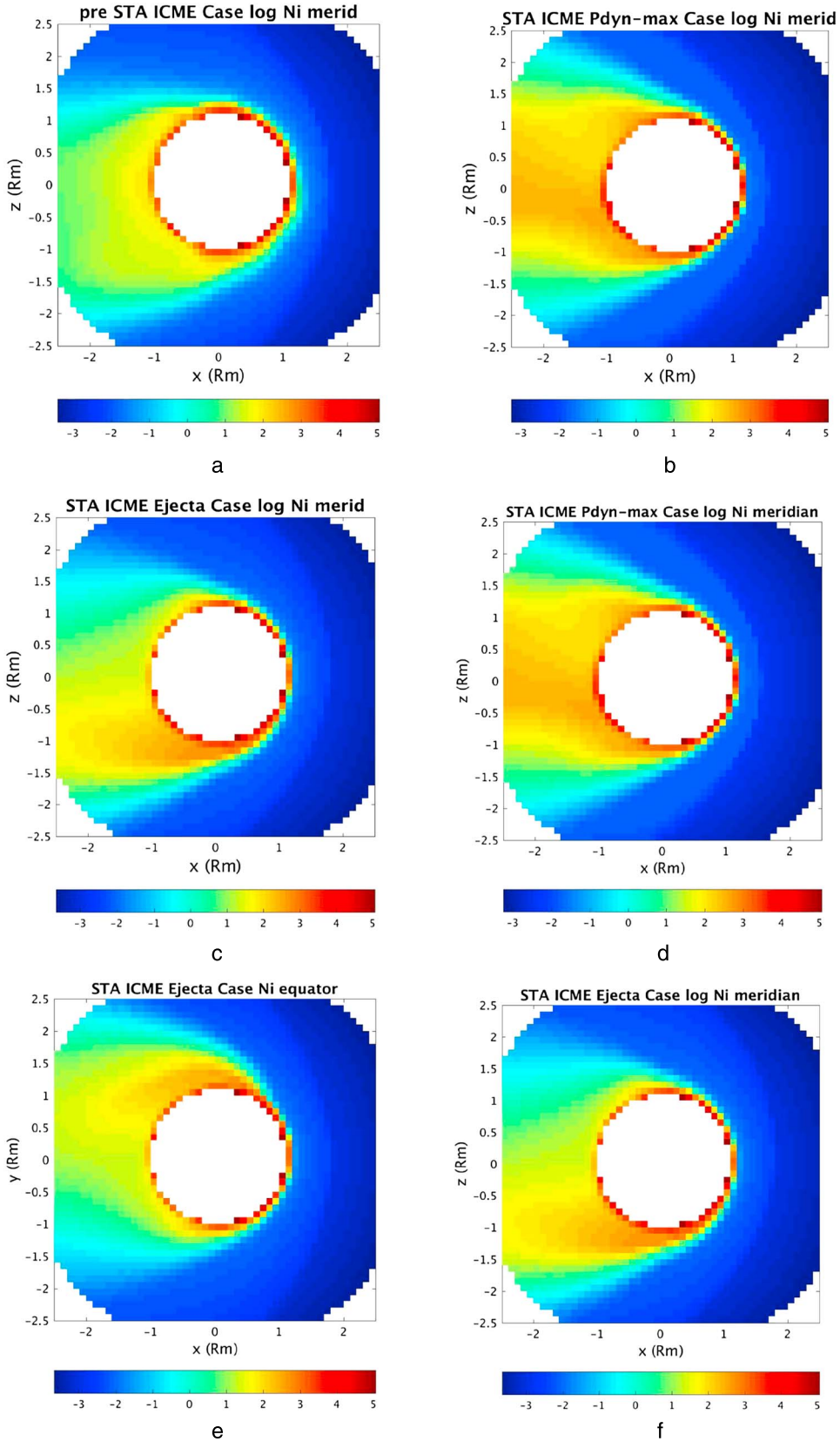

Figure 11. Same as Figure 3 but for the July 2012 event cases in Table 2. Meridian log ionospheric density contours for the three ICME phases.

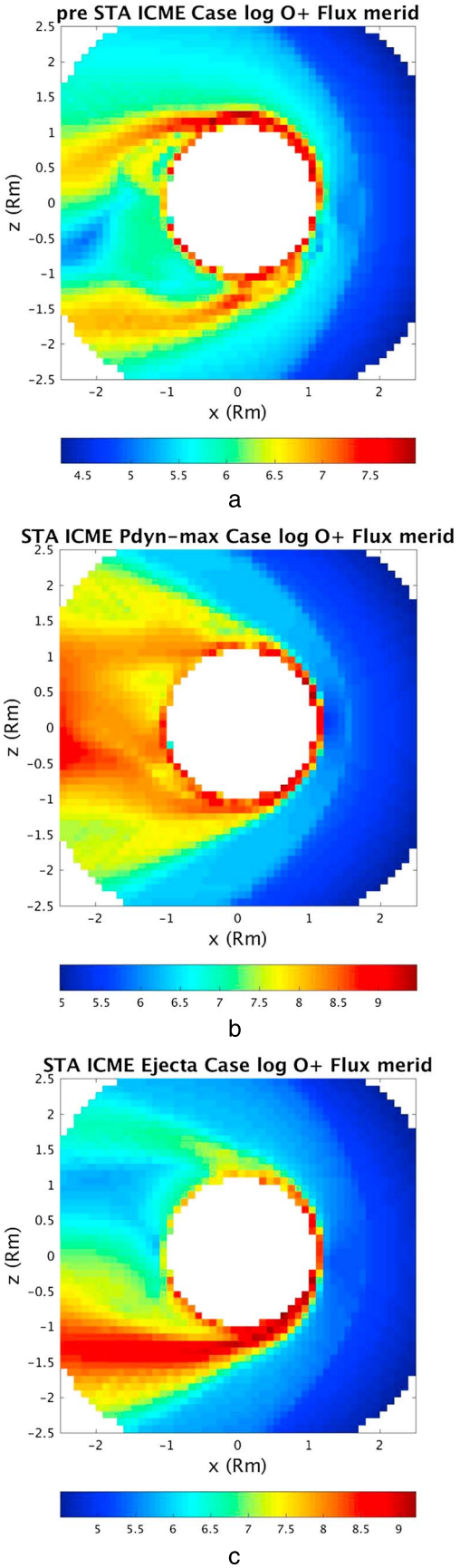

5. Discussion/Implications

In the extended mission, new observing modes have been designed to more regularly capture low-energy planetary ion outflows in the wake region. These are particularly difficult measurements to obtain due to influences of spacecraft charging, as well as limitations of fields of view and their blockages [see *McFadden et al.*, 2015]. These plans also include more wake region sampling at apoapsis (~2.3 R_m) where the cold ion wake structure is better defined. Other challenges concern the need for sufficient statistics for sorting out effects of the constantly changing crustal field and interplanetary field geometry, as well as solar wind pressure and solar EUV flux [e.g., see *Brain et al.*, 2015]. Interpreting these observations is of course an even greater challenge in ICME situations like those discussed here. Yet the more examples observed, the more we can learn.

The responses at Mars to both the March 2015 ICME, as seen on MAVEN and interpreted with solar wind interaction models, and a hypothetical more extreme case based on STEREO A observations suggest that there are patterns of behavior, as there are at Earth. Magnetic field and suprathermal electron results have already shown that the Mars-solar wind interaction is topologically different than a Venus induced interaction. The interface with the Martian obstacle is populated with open fields that channel photoelectrons from the dayside into the postterminator atmosphere and solar wind wake, and closed fields that shield part of the ionosphere [e.g., *Liemohn et al.*, 2006]. The nightside

Figure 12. Same as Figure 4 but for the July 2012 event cases in Table 2. Meridian ionospheric ion flux contours for the three ICME phases. Notice the scale changes between frames.

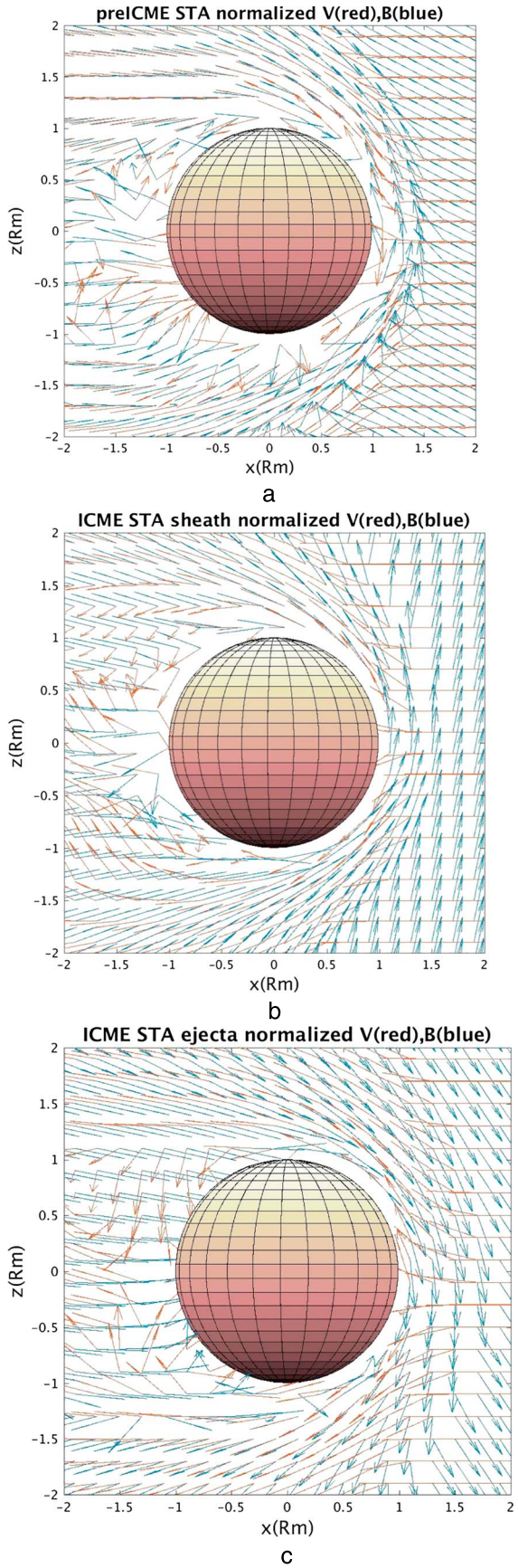

atmosphere under typical circumstances is less accessible to external electrons because the field topology is largely closed by the crustal remanent fields—even when the strongest fields are located on the dayside. Yet the magnetotail of Mars, at least to several Mars radii downstream, is filled with open fields connecting the interplanetary field to Mars on both dayside and nightside [e.g., *Brain et al.*, 2007; *Luhmann et al.*, 2015a, 2015b]. Thus, while at a distance Mars' solar wind interaction appears Venus-like, it has a number of magnetospheric features with uniquely Martian traits, including its responses to interplanetary space weather.

The idealized Mars magnetic storm, like its Earth counterpart, consists of stages defined by the different ICME stages. First, the enhanced dynamic pressure produced by solar wind plasma and field plowed up by the coronal ejecta, the ICME sheath, forces subsolar magnetosheath plasma, and field closer to Mars. This produces increased subsolar erosion of the ionosphere together with more reconnection of external and crustal fields, resulting in more open magnetic fields on the dayside. In extreme cases, the draped magnetosheath fields can be found at altitudes down to the exobase, allowing inward external field diffusion to further open the Mars magnetosphere—even on the nightside. The more open magnetosphere has many consequences from the increased access of external particles to widespread mapping of solar wind convection electric fields into the ionosphere. One can expect larger areas of diffuse auroral emissions and significant increases in related night-

Figure 13. Same as Figure 5 but for the July 2012 event experiment cases in Table 2. Meridian projections of flow (red) and field (blue) normalized model vectors. (b and c) Notice the appearance of greater outflow from low altitudes during the event.

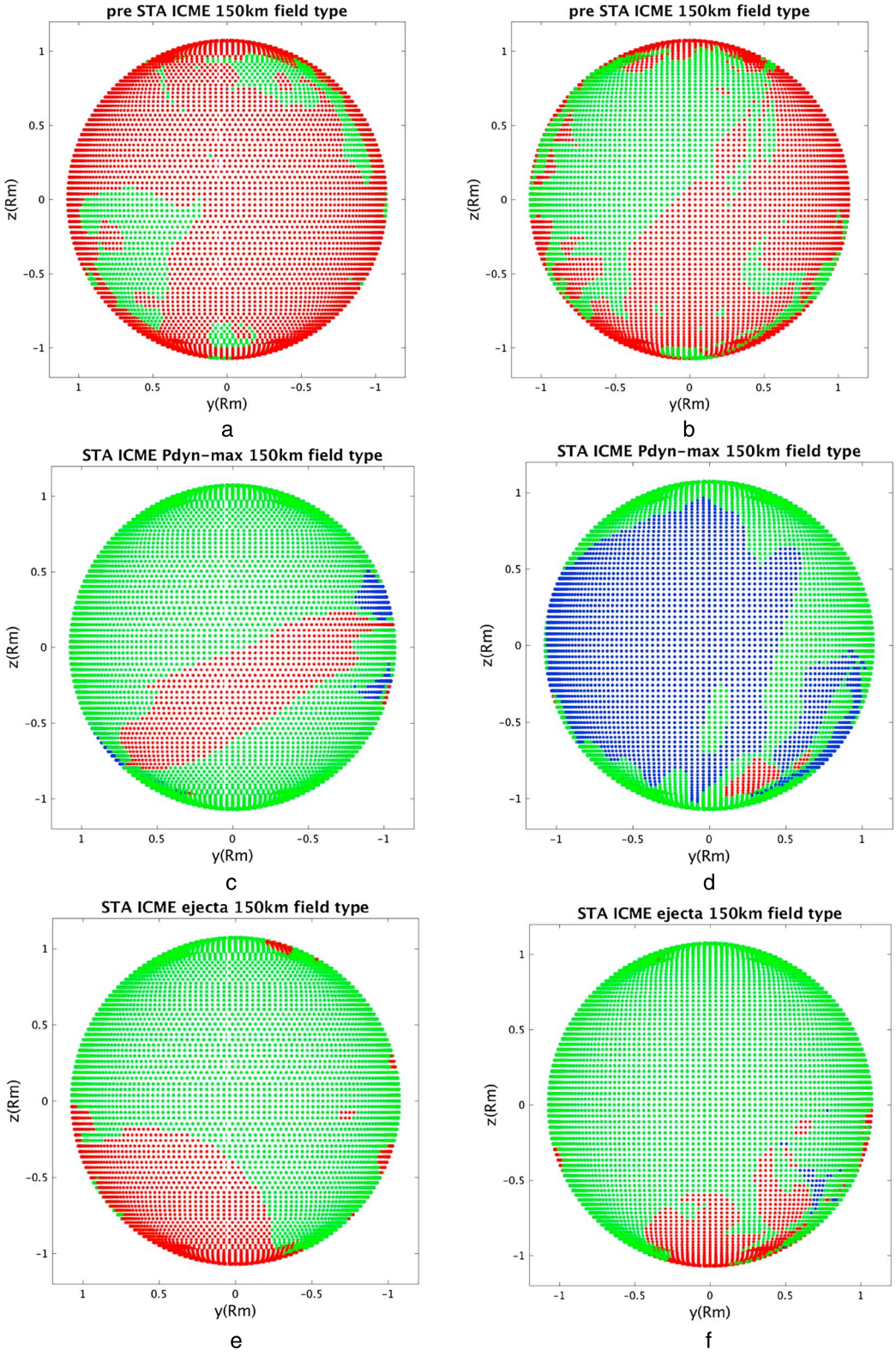

Figure 14. Same as Figure 6 but for the July 2012 event experiment at Mars. (a and b) Nightside and (e and f) dayside areas on a 150 km surface showing where the model magnetic fields are closed (red), open (green), or draped (blue). Time proceeds left to right. The large blue area on the dayside for the ICME sheath phase case, together with its field line counterpart in Figure 10, emphasizes the idea that draped, penetrated external fields can be strong drivers of atmospheric effects down to MAVEN periapsis altitudes.

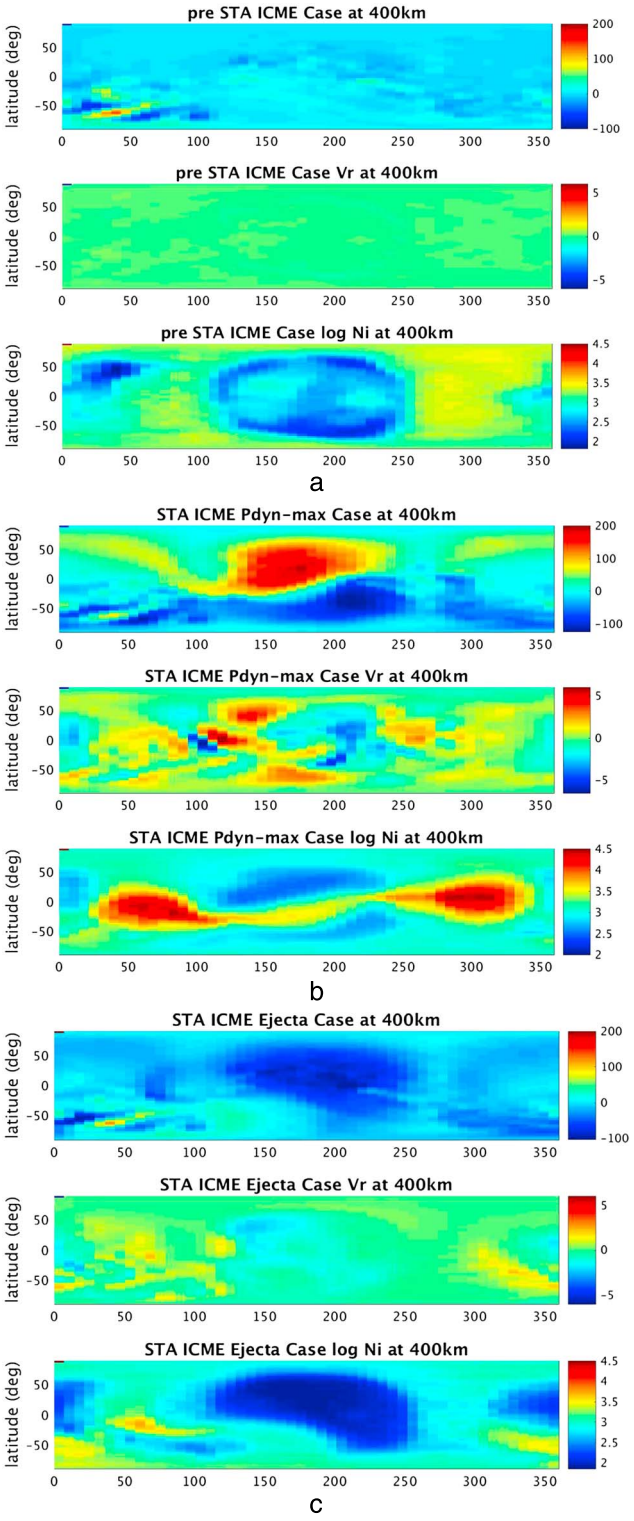

Figure 15. Same as Figure 7 but for the July 2012 extreme event experiment at Mars. The maps for 400 km altitude show the (a–c, top) vertical field, vertical velocity (a–c, middle), and (a–c, bottom) planetary heavy ion density. Both the ICME sheath and ejecta phases (Figures 15b and 15c) exhibit large deviations from the pre-event state (Figure 15a), discussed further in the text.

side ionosphere density as is observed under such conditions [e.g., *Morgan et al.*, 2014], with the more copious ionospheric outflows [e.g., *Curry et al.*, 2015]. This description can be compared to that of *Dubinin et al.* [2009] who interpreted MEX observations of the topside ionosphere during the passage of solar wind stream interaction regions, which like the ICMEs exhibit increased dynamic pressures and interplanetary magnetic field strength [see also *Edberg et al.*, 2010; *Vennerstrom*, 2011]. But while both types of solar wind disturbances can cause dayside ionosphere compression and increased solar wind penetration of the magnetic barrier, ICMEs have their own distinctive stages, and the potential to be more extreme in both duration and magnitude.

As mentioned at the outset, caveats exist regarding interpretations of the model results. For example, because the models use constant, preset atmosphere descriptions, they neglect the atmospheric effects of these events, including those related to solar and planetary particle precipitation [e.g., *Fang et al.*, 2013; *Lillis et al.*, 2012; *Lillis and Brain*, 2013; *Curry et al.*, 2015], heating, sputtering, and/or ionization related to any absorbed, energized particles, or ion drag related friction/Joule heating. The maps of atmospheric responses are simply "one-way" MHD responses of the fluid-like ionospheric ions in the model. There is also no feedback into the solar wind interaction simulation in the form of related atmospheric alteration, even though it should be expected in these cases. An exception is that increased mass loading of the incident solar wind by the pre-event atmosphere is included to the extent that additional atmospheric ion production (by impact ionization and charge exchange) occurs at lower dayside altitudes during the extreme interaction. The single fluid MHD models used here also

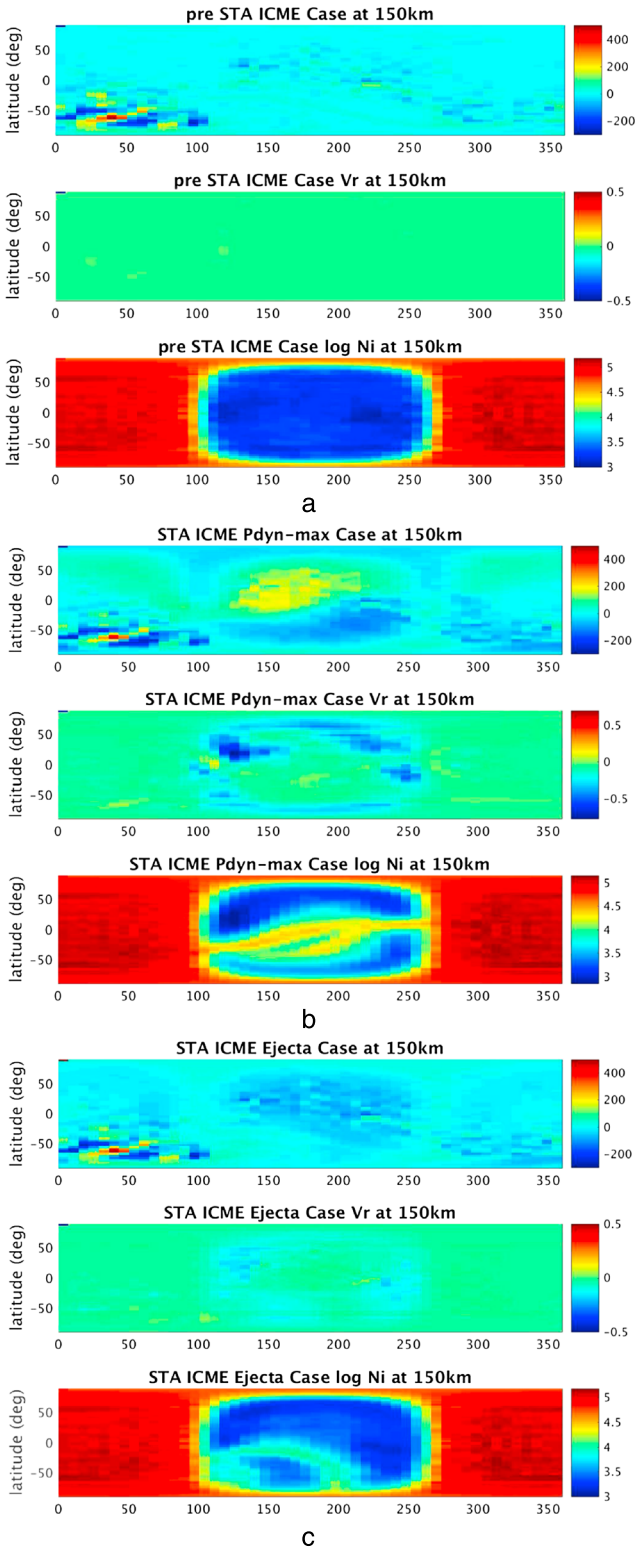

Figure 16. Same as Figure 8 but for the July 2012 event experiment at Mars. The contents are as described in Figure 15 caption above. Here strong deviations from a pre-event (a–c, top) B_r, (a–c, middle) V_r , and (a–c, bottom) planetary ion density are also seen at 150 km altitude. These can be compared with the relatively modest response at this altitude seen in Figure 8 for the March 2015 event.

do not include effects of the more kinetic, high-altitude heavy ions that are spatially divided into escaping and impacting populations [e.g., *Curry et al*., 2015], affecting their total fluxes and balance of composition. The MHD simulations also do not include processes involving wave-particle interactions like the perpendicular acceleration of heavy ions that occurs in Earth's auroral zone in response to auroral electron precipitation, or alterations of electron temperatures at the solar wind interaction boundary by Venus-like current-driven plasma instabilities there [e.g., *Strangeway and Russell*, 1996]. In addition, as the reconnection process in the simulations is determined by numerical diffusion, it is mainly the successful data comparisons that validate that approximation. In the extreme events the reconnection is occurring at altitudes where the resistivity due to ion-neutral collisions becomes important, a transition that may have consequences not yet explored. Finally, any special ion losses related to short timescale ICME features such as the leading shock, or sudden field rotations/current sheets in the passing structure, have not been considered here nor is the possibility of alteration of the plasma interaction by an event-related change in the inner boundary condition used in the models, e.g., significant penetration of interplanetary field into the planetary interior. In other words, the numerical experiment for the July 2012 event described here is only an initial foray into investigating its potential effects.

6. Concluding Remarks

Mars, with its combination of a significant ionosphere and crustal magnetic fields, experiences a unique solar wind interaction among the terrestrial planets. This difference includes its response to the space weather events, ICMEs, which cause geomagnetic storms at Earth. In this

study we investigated some of the phenomena associated with these Martian magnetic storms, including magnetic topology changes and ionospheric disturbances. Because the MAVEN observations of these types of conditions are still limited, we use a data-validated (BATS-R-US) MHD model as an investigative tool. In particular, the simulations previously used to estimate the global ion escape rate enhancement caused by a March 2015 event [see *Jakosky et al*., 2015a] is more closely examined and then applied to a similar study of Mars' response to a much stronger hypothetical event based on an extreme ICME observed on STEREO A in July 2012. As expected, the latter produced more extreme effects including more extensive penetration of the external magnetic fields into the atmosphere, and a more energized ionosphere resulting in enhanced ion outflows.

The broader implications of these analyses relate to the overall importance of the solar wind at Mars. If the solar wind interaction represents a sufficient source of energy input to the atmosphere, today and over time, it cannot be neglected in either current observations and models or historical reconstructions of Mars' evolutionary path. For conditions in the space environment that are typical today, such as those witnessed on MAVEN during the March 2015 ICME passage, the effects on consequences such as atmospheric ion escape rates are detectable but modest in terms of their ability to alter the Mars atmosphere and climate over several billion years [e.g., *Brain et al*., 2015]. Nevertheless, other evidence including observed isotope ratios [see *Slipski and Jakosky*, 2016] argues for a much higher rate of atmosphere escape in the past, enabled by nonphotochemical and nonthermal processes. The existence of higher solar EUV fluxes and a more active Sun in the early solar system, inferred from observations of younger Sun-like stars, would have affected the importance of solar wind interaction influences on the atmosphere. The simulation of an extreme solar event described here provides a realistic example of such conditions, albeit by today's standards, and for today's conditions at Mars and on the Sun. Many historical extrapolations of solar wind interaction effects [e.g., *Luhmann et al*., 1992; *Lammer et al*., 2013] have assumed continuous enhancements of ambient solar and interplanetary conditions going back in time. The reality is likely to have involved increased frequency of coronal transients, which changes the perception—if not the outcome—of the solar wind interaction contribution. As knowledge of magnetic activity and space environments of younger Sun-like stars increases with new observations [e.g., *Wood*, 2014], it will become clearer whether transient events should (or can) be invoked to explain key evolutionary evidence. In the meantime, the Interior Exploration using Seismic Investigations, Geodesy, and Heat Transport mission is scheduled to carry a magnetometer to the surface soon. Those measurements will provide a definitive measure and test of the penetrating power of magnetic storms at Mars.

Acknowledgments

This work makes use of the BATS-R-US MHD model developed at the University of Michigan under the direction of T. Gombosi, with the Mars-solar wind interaction application developed there by coauthor Y-J. Ma as part of a PhD research project. The numerical simulations were carried out using NASA computing facilities at ARC. The MAVEN data shown are archived in NASA's Planetary Data System (PDS). The STEREO data are archived and accessible through the Space Physics Data Facility at the NSSDC. The July 2012 STEREO A derived plasma parameters were provided to Y. Liu by the PLASTIC investigation team at UNH (PI A.B. Galvin) for the Nature Communications publication referenced below. This research has been supported by NASA through MAVEN Project subcontracts to the authors, managed by LASP, University of Colorado, under the direction of MAVEN PI B.M. Jakosky. C. F. Dong is supported by the NASA Living With a Star Jack Eddy Postdoctoral Fellowship Program, administered by the University Corporation for Atmospheric Research.

References

Acuna, M. H., et al. (1998), Magnetic fields and plasma observations at Mars: Initial results of the Mars Global Surveyor mission, *Science*, *279*, 1670–1676, doi:10.1126/science.279.5357.1670a.

Aran, A., D. Lario, B. Sanahuja, R. G. Marsden, M. Dryer, C. D. Fry, and S. M. P. McKenna-Lawlor (2007), Modeling and forecasting solar energetic particle events at Mars: The event on 6 March 1989, *Astron. Astrophys.*, *469*, 1123–1134, doi:10.1051/0004-6361:20077233.

Brain, D. A., F. Bagenal, M. H. Acuna, and J. E. P. Connerney (2003), Martian magnetic morphology: Contributions from the solar wind and crust, *J. Geophys. Res.*, *108*(A12), 1424, doi:10.1029/2002JA009482.

Brain, D. A., J. S. Halekas, R. Lillis, D. L. Mitchell, and R. P. Lin (2005), Variability of the altitude of the Martian magnetosheath, *Geophys. Res. Lett.*, *32*, L18203, doi:10.1029/2005GL023126.

Brain, D. A., R. Lillis, D. L. Mitchell, J. S. Halekas, and R. P. Lin (2007), Electron pitch angle distributions as indicators of magnetic field topology near Mars, *J. Geophys. Res.*, *112*, A09201, doi:10.1029/2007JA012435.

Brain, D. A., et al. (2015), The spatial distribution of planetary ion fluxes near Mars observed by MAVEN, *Geophys. Res. Lett.*, *42*, 9142–9148, doi:10.1002/2015GL065293.

Connerney, J. E. P., J. Espley, P. Lawton, S. Murphy, J. Odom, R. Oliversen, and D. Sheppard (2015), The MAVEN magnetic field investigation, *Space Sci. Rev.*, *195*, 257–291, doi:10.1007/s11214-015-0169-4.

Crider, D. H., J. Espley, D. A. Brain, D. L. Mitchell, J. E. P. Connerney, and M. H. Acuna (2005), Mars Global Surveyor observations of the Halloween 2003 solar superstorm's encounter with Mars, *J. Geophys. Res.*, A09S21, doi:10.1029/2004JA010881.

Curry, S. M., et al. (2015), Response of Mars O^+ pickup ions to the 8 March 2015 ICME: Inferences from MAVEN data-based models, *Geophys. Res. Lett.*, *41*, 9095–9102, doi:10.1002/2015GL065304.

Delory, G. T., J. G. Luhmann, D. Brain, R. J. Lillis, D. L. Mitchell, R. A. Mewaldt, and T. V. Falkenberg (2012), Energetic particles detected by the Electron Reflectometer instrument on Mars Global Surveyor, 1999–2006, *Space Weather*, *10*, S06003, doi:10.1029/2012SW000781.

Dong, C. F., et al. (2015), Multifluid MHD study of the solar wind interaction with Mars' upper atmosphere during the 2015 March 8th ICME event, *Geophys. Res. Lett.*, *42*, 9103–9112, doi:10.1002/2015GL065944.

Dubinin, E., M. Fraenz, J. Woch, F. Duru, D. Gurnett, R. Modolo, S. Barabash, and R. Lundin (2009), Ionospheric storms on Mars: Impact of the corotating interaction region, *Geophys. Res. Lett.*, *36*, L01105, doi:10.1029/2008GL036559.

Dungey, J. W. (1968), The reconnection model of the magnetosphere, in *Earth's Particles and Fields*, pp. 385–392, Reinhold Books, New York.

Edberg, N. J. T., H. Nilsson, A. O. Williams, M. Lester, S. E. Milan, S. W. H. Cowley, M. Fraenz, S. Batabash, and Y. Futaana (2010), Pumping out the atmosphere of Mars through solar wind pressure pulses, *Geophys. Res. Lett.*, *37*, L03107, doi:10.1029/2009GL041814.

Fang, X., S. W. Bougher, R. E. Johnson, J. G. Luhmann, Y.-J. Ma, Y.-C. Wang, and M. W. Liemohn (2013), The importance of pickup oxygen ion precipitation in the Mars upper atmosphere under extreme solar wind conditions, *Geophys. Res. Lett.*, *40*, 1922–1927, doi:10.1002/grl.50415.

Futaana, Y., et al. (2008), Mars Express and Venus Express multipoint observations of geoeffective flare events in December 2006, *Planet. Space Sci.*, *56*, 873–880, doi:10.1016/j.pss.2007.10.014.

Halekas, J., E. Taylor, G. Dalton, G. Johnson, D. Curtis, J. McFadden, D. Mitchell, R. Lin, and B. Jakosky (2013), The solar wind analyzer for MAVEN, *Space Sci. Rev.*, 1–27.

Jakosky, B. M., et al. (2015a), MAVEN observations of the response of Mars to an interplanetary coronal mass ejection from the Sun, *Science*, *350*, doi:10.1126/science.aad0210.

Jakosky, B. M., et al. (2015b), The Mars Atmosphere and Volatile EvolutioN (MAVEN) mission, *Space Sci. Rev.*, 1–46.

Lammer, H., et al. (2013), Outgassing history and escape of the Martian atmosphere and water inventory, *Space Sci. Rev.*, *174*, 113–154, doi:10.1007/s11214-012-9943-8.

Lee, C. O., et al. (2017), MAVEN observations of the solar cycle 24 space weather conditions at Mars, *J. Geophys. Res. Space Physics*, *122*, doi:10.1002/2016JA023495, in press.

Li, Y., J. G. Luhmann, B. J. Lynch, and E. K. J. Kilpua (2014), Magnetic clouds and origins in STEREO era, *J. Geophys. Res. Space Physics*, *119*, 3237–3246, doi:10.1002/2013JA019538.

Liemohn, M. W., Y. Ma, R. A. Frahm, X. Fang, J. U. Kozyra, A. F. Nagy, J. D. Winningham, J. R. Sharber, S. Barabash, and R. Lundin (2006), Mars global MHD predictions of magnetic connectivity between the dayside ionosphere and the magnetospheric flanks, *Space Sci. Rev.*, 63–76.

Lillis, R. J., and D. A. Brain (2013), Nightside electron precipitation at Mars: Geographic variability and dependence on solar wind conditions, *J. Geophys. Res. Space Physics*, *118*, 3546–3556, doi:10.1002/jgra.50171.

Lillis, R. J., D. A. Brain, G. T. Delory, D. L. Mitchell, J. G. Luhmann, and R. P. Lin (2012), Evidence for suprathermal secondary electrons produced by SEP ionization in the Martian atmosphere, *J. Geophys. Res.*, *117*, E03004, doi:10.1029/2011JE003932.

Liu, Y., et al. (2014), Observations of an extreme storm in interplanetary space caused by successive coronal mass ejections, *Nat. Commun.*, *5*, doi:10.1038/ncomms4481.

Luhmann, J. G., R. E. Johnson, and M. H. G. Zhang (1992), Evolutionary impact of sputtering of the Martian atmosphere by O^+ pickup ions, *Geophys. Res. Lett.*, *19*, 2151–2154, doi:10.1029/92GL02485.

Luhmann, J. G., Y. J. Ma, D. A. Brain, D. Ulusen, R. J. Lillis, J. S. Halekas, and J. R. Espley (2015a), Solar wind interaction effects on the magnetic fields around Mars: Consequences for interplanetary and crustal field measurements, *Planet. Space Sci.*, *117*, 15–23, doi:10.1016/j.pss.2015.05.004.

Luhmann, J. G., et al. (2015b), Implications of MAVEN Mars near-wake measurements and models, *Geophys. Res. Lett.*, *42*, 9087–9094, doi:10.1002/2015GL066122.

Ma, Y.-J., and A. F. Nagy (2007), Ion escape fluxes from Mars, *Geophys. Res. Lett.*, *34*, L08201, doi:10.1029/2006GL029208.

Ma, Y.-J., A. F. Nagy, I. V. Sokolov, and K. C. Hansen (2004), Three-dimensional, multispecies, high spatial resolution MHD studies of the solar wind interaction with Mars, *J. Geophys. Res.*, *109*, A07211, doi:10.1029/2003JA010367.

Ma, Y.-J., X. Futaana, C. T. Russell, A. F. Nagy, G. Toth, J. G. Luhmann, D. A. Brain, and C. Dong (2014), Effects of crustal field rotation on the solar wind plasma interaction with Mars, *Geophys. Res. Lett.*, *41*, 6563–6569, doi:10.1002/2014GL060785.

Ma, Y.-J., et al. (2015), MHD model results of solar wind interaction with Mars and comparison with MAVEN plasma observations, *Geophys. Res. Lett.*, *42*, 9113–9120, doi:10.1002/2015GL065218.

Ma, Y.-J., et al. (2017), Variations of the Martian plasma environment during the ICME passage on 8 March 2015: A time-dependent MHD study, *J. Geophys. Res. Space Physics*, *122*, 1714–1730, doi:10.1002/2016JA023402.

Manucci, A. J., B. T. Tsurutani, B. A. Iijima, A. Komjathy, A. Saito, W. D. Gonzalez, F. L. Guarnieri, J. U. Kozyra, and R. Skoug (2005), Dayside global ionospheric response to the major interplanetary events of October 29–30, 2003 "Halloween Storms", *Geophys. Res. Lett.*, *32*, L12S02, doi:10.1029/2004GL021467.

McFadden, J. P., et al. (2015), MAVEN suprathermal ion and thermal ion composition (STATIC) instrument, *Space Sci. Rev.*, *195*, 199–256, doi:10.1007/s11214-015-0175-6.

McKenna-Lawlor, S., M. Dryer, C. D. Fry, W. Sun, D. Lario, C. S. Deehr, B. Sanahuja, V. A. Afonin, M. I. Verigin, and G. A. Kotova (2005), Predictions of energetic particle radiation in the close Martian environment, *J. Geophys. Res.*, *110*, A03102, doi:10.1029/2004JA010587.

Mitchell, D. L., R. P. Lin, C. Mazelle, H. Rème, P. A. Cloutier, J. E. P. Connerney, M. H. Acuña, and N. F. Ness (2001), Probing Mars' crustal magnetic field and ionosphere with the MGS Electron Reflectometer, *J. Geophys. Res.*, *106*(E), 23,419–23,428, doi:10.1029/2000JE001435.

Moore, T. E., and G. V. Khazanov (2010), Mechanisms of ionospheric mass escape, *J. Geophys. Res.*, *115*, A00J13, doi:10.1029/2009JA014905.

Morgan, D. D., et al. (2014), Effects of a strong ICME on the Martian ionosphere as detected by Mars Express and Mars Odyssey, *J. Geophys. Res. Space Physics*, *119*, 5891–5908, doi:10.1002/2013JA019522.

Neugebauer, M., R. Goldstein, and B. E. Goldstein (1997), Features observed in the trailing regions of interplanetary clouds from coronal mass ejections, *J. Geophys. Res.*, *102*, 19,743–19,752, doi:10.1029/97JA01651.

Opgenoorth, H. J., D. J. Andrews, M. Fraenz, M. Lester, N. J. T. Edberg, D. Morgan, F. Duru, O. Witasse, and A. O. Williams (2013), Mars ionosphere response to solar wind variability, *J. Geophys. Res. Space Physics*, *118*, 6558–6587, doi:10.1002/jgra.50537.

Opitz, A., A. Fedorov, P. Wurz, J. A. Sauvaud, R. Karrer, A. B. Galvin, S. Barabash, and F. Ipavich (2010), Solar wind bulk velocity throughout the inner heliosphere from multispacecraft measurements, *Sol. Phys.*, *264*, 377–382, doi:10.1007/s11207-010-9583-7.

Schneider, N. M., et al. (2015), Discovery of diffuse aurora on Mars, *Science*, *350*, doi:10.1126/science.aad0313.

Schwenn, R. (2006), Space weather: The solar perspective, *Living Rev. Sol. Phys.*, *3*(2), doi:10.12942/lrsp-2006-2.

Shprits, Y., D. Subbotin, B. Ni, R. Horne, D. Baker, and P. Cruce (2011), Profound change of the near-Earth radiation environment caused by solar superstorms, *Space Weather*, *9*, S08007, doi:10.1029/2011SW000662.

Slipski, M., and B. M. Jakosky (2016), Argon isotopes as tracers for Martian atmospheric loss, *Icarus*, *272*, 212–227, doi:10.1016/j.icarus.2016.02.047.

Strangeway, R. J., and C. T. Russell (1996), Plasma waves and field aligned currents in the Venus plasma mantle, *J. Geophys. Res.*, *101*, 17,313–17,324, doi:10.1029/96JA00927.

Strangeway, R. J., R. E. Ergun, Y. J. Su, C. W. Carlson, and R. C. Elphic (2005), Factors controlling ionospheric outflows as observed at intermediate altitudes, *J. Geophys. Res.*, *110*, A03221, doi:10.1029/2004JA010829.

Ulusen, D., J. G. Luhmann, Y. Ma, and D. A. Brain (2016), Solar control of the Martian magnetic topology: Implications from model-data comparisons, *Planet. Space Sci.*, *128*, 1–13, doi:10.1016/j.pss.2016.01.007.

Vennerstrom, S. (2011), Magnetic storms on Mars, *Icarus*, *215*, 234–241, doi:10.1016/j.icarus.2011.06.030.

Vennerstrom, S., et al. (2016), Extreme geomagnetic storms, *Sol. Phys.*, *291*, 1447–1481, doi:10.1007/s11207-016-0897-y.

Verigin, M. I., et al. (2004), Unusually distant bow shock encounters at Mars: Analysis of March 24, 1989 event, *Space Sci. Rev.*, *111*, 233–243, doi:10.1023/B:SPAC.0000032713.86796.d1.

Wood, B. E. (2014), Evidence for a weak wind from the young Sun, *Astrophys. J. Lett.*, *781*, doi:10.1088/2041-8205/781/2/L33.

Zhang, M. H. G., and J. G. Luhmann (1992), Comparisons of peak ionosphere pressures at Mars and Venus with incident solar wind dynamic pressure, *J. Geophys. Res.*, *97*, 1017–1025, doi:10.1029/91JE02721.

Zhang, T.-L., et al. (2008), Venus Express observations of an atypically distant bow shock during the passage of an interplanetary coronal mass ejection, *J. Geophys. Res.*, *113*, E00B12, doi:10.1029/2008JE003128.